LIMNOLOGY
and
OCEANOGRAPHY

ASLO

Limnol. Oceanogr. 62, 2017, S112–S130

doi: 10.1002/lno.10646

Responses of carbonate system and CO_2 flux to extended drought and intense flooding in a semiarid subtropical estuary

Hongming Yao, Xinping Hu *

Department of Physical and Environmental Science, Texas A&M University - Corpus Christi, Corpus Christi, Texas

Abstract

Globally, estuaries are considered important CO_2 sources to the atmosphere. However, estuarine water carbonate chemistry and CO_2 flux studies have focused on temperate and high latitude regions, leaving a significant data gap in subtropical estuaries. In this study, we examined water column carbonate system and air–water CO_2 flux in the Mission-Aransas Estuary, a subtropical semiarid estuary in the northwestern Gulf of Mexico, by collecting samples at five System Wide Monitoring Program stations from 05/2014 to 04/2015. The carbonate system parameters (total alkalinity [TA], dissolved inorganic carbon [DIC], pH, CO_2 partial pressure [pCO_2], and carbonate saturation state with respect to aragonite [Ω_{Ar}]) and air–water CO_2 flux all displayed substantial seasonal and spatial variations. Based on freshwater inflow conditions, a drought period occurred between 05/2014 and 02/2015, while a flooding period occurred from 03/2015 to 04/2015. Average DIC was 2194.7 ± 156.8 μmol kg^{-1} and 2132.5 ± 256.8 μmol kg^{-1}, TA was 2497.6 ± 172.1 μmol·kg^{-1} and 2333.4 ± 283.1 μmol kg^{-1}, pCO_2 was 477 ± 94 μatm and 529 ± 251 μatm, and CO_2 flux was 28.3 ± 18.0 mmol C·m^{-2}·d^{-1} and 51.6 ± 83.9 mmol·C·m^{-2}·d^{-1} in the drought and flooding period, respectively. Integrated annual air–water CO_2 flux during our studied period was estimated to be 12.4 ± 3.3 mol·C·m^{-2}·yr^{-1}, indicating that this estuary was a net CO_2 source. High wind speed, warm climate, riverine input, and estuarine biogeochemical processes all contributed to the high CO_2 efflux despite the modest pCO_2 levels year round.

Human activities have significantly increased atmospheric CO_2 concentration since the Industrial Revolution. Although occupying a small area (approximately 0.3%) of the global ocean, estuaries play a disproportionately important role in the global CO_2 budget (Bauer et al. 2013). In general, estuaries are a net CO_2 source due to net heterotrophy. For example, Frankignoulle (1998) suggested that CO_2 efflux from European estuaries represents 5–10% of anthropogenic CO_2 emissions throughout Europe. Global estuarine CO_2 emissions could reach an approximate rate of 0.1–0.25 Pg·C·yr^{-1}, which is on the same order of magnitude as continental shelf CO_2 uptake and equivalent to as much as 30% of total riverine carbon export (Zhai et al. 2007; Cai 2011; Bauer et al. 2013; Chen et al. 2013; Regnier et al. 2013; Laruelle et al. 2015). Large CO_2 release from estuaries could be attributed to hydrologic conditions (i.e., due to higher dissolved inorganic carbon [DIC] to alkalinity ratio in river waters than the receiving seawater) and intensive biological activities. For example, Joesoef et al. (2015) found that more CO_2 is released into the atmosphere in the upper Delaware estuary than the lower estuary, and Guo et al. (2009) reported that CO_2 flux in the Pear River Estuary is dominated by aerobic remineralization of organic matter.

There are many uncertainties in estimating CO_2 flux in an estuary. A major reason for such uncertainty is temporal variation of riverine fluxes (Abril et al. 2004; Crosswell et al. 2014) that are not easily captured in estuarine studies, which tend to have low temporal sampling resolution. On the other hand, despite that lagoonal estuaries are generally recognized as important CO_2 sources particularly in tropical and temperate areas (Laruelle et al. 2010), whether the existing global estimate in those studied areas can represent all estuarine types is unknown given the drastically different hydrologic conditions of these estuaries. As one of the world's largest subtropical lagoonal estuary systems (Dürr et al. 2011), the northwestern Gulf of Mexico (GOM) estuaries lack data for studying the CO_2 source/sink issue. Located in a semiarid subtropical region, south Texas has been

*Correspondence: xinping.hu@tamucc.edu

Special Issue: Headwaters to Oceans: Ecological and Biogeochemical Contrasts Across the Aquatic Continuum
Edited by: Marguerite Xenopoulos, John A. Downing, M. Dileep Kumar, Susanne Menden-Deuer, and Maren Voss

experiencing prolonged drought with intense flooding occurring intermittently, thus estuaries in this area receive generally low riverine inflows, punctuated by large storms (Milliman et al. 2008; Mooney and McClelland 2012). How the changing hydrologic state alters CO_2 flux and its magnitude is unclear.

In an estuary, carbonate system parameters are usually controlled by mixing and biogeochemical processes. An estuary that receives variable nutrient and organic matter input from a river will have altered metabolic processes, which will affect the carbonate system (Doney et al. 2009; Feely et al. 2010). For example, in the Chwaka Bay of Tanzania, due to the presence of seagrass, pH increases and total DIC decreases through enhanced photosynthesis and calcification (Semesi et al. 2009); while in the Long Island Sound, significant pH reduction could occur when enhanced respiration in subsurface water is coupled with CO_2 production (Wallace et al. 2014). In estuaries with significant freshwater influence, carbonate saturation state with respect to aragonite (Ω_{Ar}) is strongly correlated with salinity. For example, in Glacier Bay in the eastern Gulf of Alaska, low total alkalinity (TA) concentration, resulting from glacier discharge, decreases Ω_{Ar} substantially to below aragonite undersaturation (Reisdorph and Mathis 2014). The carbonate system parameters in high latitude estuaries have large fluctuations due to significant seasonal changes in freshwater flux, nutrient delivery, and light intensity (Cross et al. 2013; Reisdorph and Mathis 2014). Even in a single estuary, carbonate system parameters could change quickly because of varying riverine input and strength of biological activities, as well as weather conditions (Mooney and McClelland 2012).

In this study, we characterized carbonate chemistry and CO_2 flux in the Mission-Aransas Estuary (MAE). Our primary goals were to understand how the carbonate system in MAE responded to freshwater input, and to study the air–water CO_2 flux in this estuary and understand its control(s).

Materials and methods

Field sampling

MAE is a shallow lagoonal estuary located along the south Texas coast in the northwestern GOM (Fig. 1). It consists of three connected water bodies: Aransas Bay is a defined as a primary bay and is connected to the GOM via the Aransas ship channel; Copano and Mesquite are secondary bays closer to riverine input (Kim and Montagna 2012). Copano Bay receives freshwater inflows directly from the Mission and Aransas Rivers, the two major freshwater sources for the entire estuary. Mesquite Bay receives inflow from adjacent San Antonio Bay during flooding periods.

Five long-term System Wide Monitoring Program (SWMP) stations were established in the MAE by the Mission-Aransas National Estuarine Research Reserve (MA-NERR) in 2007 (Fig. 1, https://sites.cns.utexas.edu/manerr). The SWMP program is a nationally coordinated and standardized program and is used for tracking short-term variability and long-term changes in a host of biological, physical, and chemical parameters. The five stations were designed to represent key estuarine conditions that range from freshwater inflow (station CW in Fig. 1) to hydrologic connection between the estuary and the GOM (SC; Evans et al. 2015). Water depths at these sampling stations ranged from 1.2 m (MB) to 6.2 m (SC).

Surface and bottom water samples were taken by a Van Dorn water sampler during the 05/2014–04/2015 period following the standard protocol for ocean CO_2 studies (Dickson et al. 2007). From 11/2014 to 03/2015, samples were taken monthly, and sampling occurred biweekly during the warmer months in the rest of our sampling year. All field samplings were done between 09:00 h and 14:00 h. Briefly, 250 mL narrow-neck borosilicate glass bottles were used to collect water samples for TA, DIC, and pH analyses. 100 μL of saturated $HgCl_2$ was added to the water sample to arrest biological activity. The samples were stored at 4°C in the dark until analysis, usually within 2–3 weeks of sample collection. One hundred twenty-five milliliters polypropylene bottles were used to collect Ca^{2+} samples. In the study by Bockmon and Dickson (2014), filtration for coastal water carbonate system characterization was recommended. However, we did not find significant difference between filtered and unfiltered samples in this estuary (also see Hu et al. 2015), thus we used unfiltered samples for this study. A calibrated YSI 6600 V2 data sonde was used to obtain in situ temperature, pressure, and dissolved oxygen (DO) concentration at each station.

To examine the effect of freshwater inflow on the estuarine carbonate system, we imported daily discharge data from the United States Geological Survey (USGS) real-time stream flow record (http://waterdata.usgs.gov/tx/nwis/rt) for Mission (USGS #08189500) and Aransas Rivers (USGS #08189700), then calculated monthly riverine discharge. Wind speed and barometric pressure were obtained every 30 min from the weather station at Copano East (CE) (http://lighthouse.tamucc.edu/pq), and daily mean wind speed was applied to sampling days. Wind speed data collected from the weather station (3 m) was converted to 10 m above the water surface using the wind profile power law,

$$\frac{u_1}{u_2} = \left(\frac{z_1}{z_2}\right)^P \quad (1)$$

here u_2 is the wind speed at height $z_2 = 10$ m, u_1 is the collected wind speed data at height $z_1 = 3$ m, the exponent P (0.11) around GOM area is extracted by Hsu et al. (1994; $p = 0.11$).

Chemical analyses

All water samples were analyzed for DIC, TA, pH, and salinity. Ca^{2+} was analyzed for surface water only. For DIC analysis, 0.5 mL water sample was acidified by 0.5 mL 10% H_3PO_4 using a 2.5 mL syringe pump. The released CO_2 was

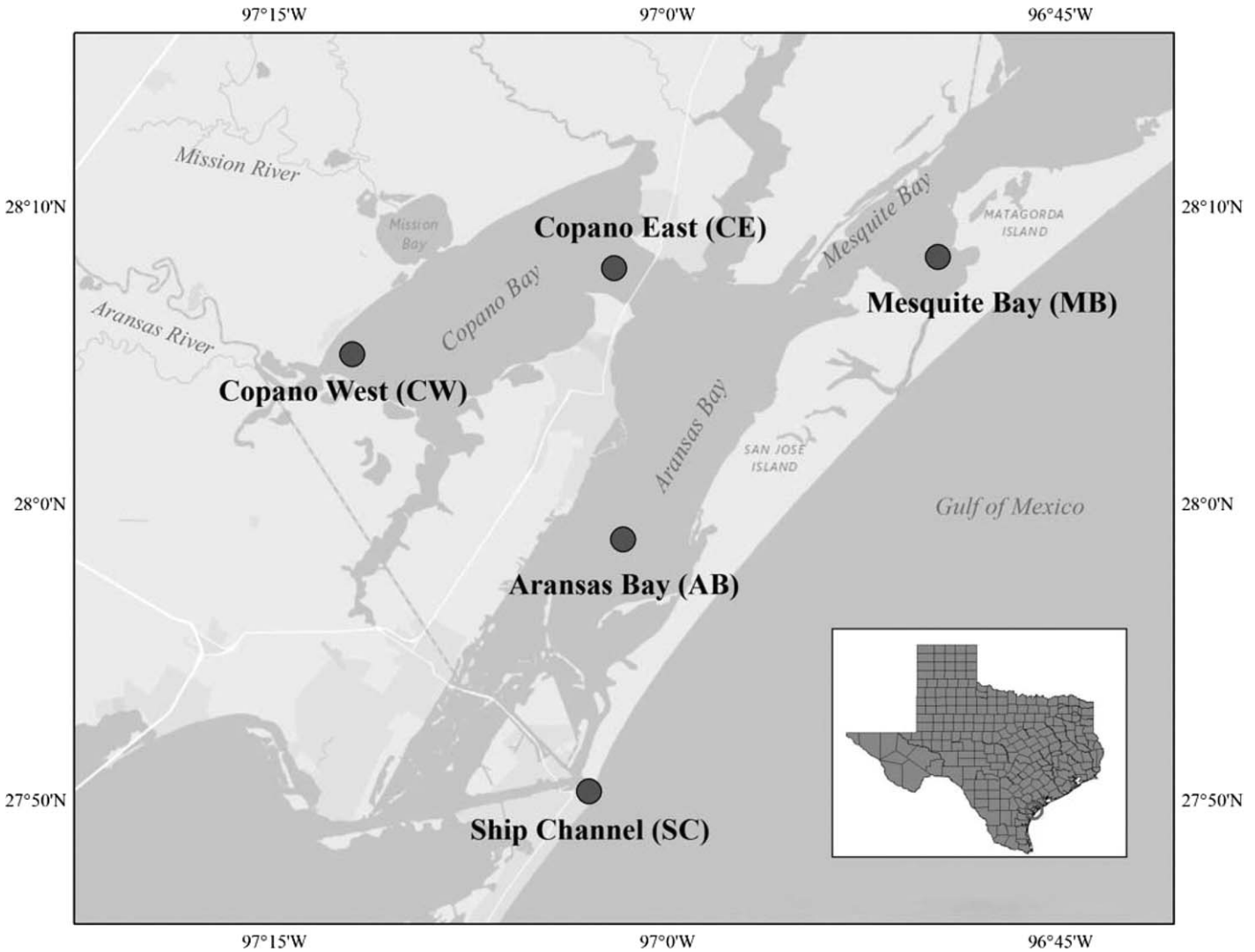

Fig. 1. The map of the Mission-Aransas Estuary (MAE) and the five System Wide Monitoring Program stations.

analyzed on an AS-C3 DIC analyzer (Apollo SciTech). To analyze TA, 25 mL water sample was titrated with a 0.1 M HCl solution (in 0.5 M NaCl) using an AS-ALK2 alkalinity titrator (Apollo SciTech). Temperature of the titration vessel was maintained at 22 ± 0.1°C using a water-jacketed circulation system. Certified Reference Material or CRM (Dickson et al. 2003) was used to construct the standard curve for the DIC analysis and to calibrate the acid used for TA titration. DIC and TA analyses had a precision of ± 0.1%.

A spectrophotometric method (Carter et al. 2013) using purified m-cresol purple (mCP) obtained from Dr. Robert Byrne's lab (University of South Florida) was used for pH analysis on total scale (Liu et al. 2011). The indicator was adjusted to pH 7.92 ± 0.01 every time before sample analysis with the aid of a calibrated Orion™ Ross™ glass electrode. A 10-cm water-jacketed absorbance cell used for pH measurements (Carter et al. 2013) was kept at 25 ± 0.01°C. The dye effect was corrected via duplicate runs of each sample by adding two volumes (30 μL and 60 μL) of mCP following the procedure in Clayton and Byrne (1993). This method had a precision of ± 0.0004 pH unit. Because of salinity limitations of the spectrophotometric method (20–40, Liu et al. 2011), for lower salinity samples we used the calibrated pH electrode to measure pH at 25°C. All pH values obtained using the potentiometric method were converted to total scale using temperature and salinity (Millero 2001).

Salinity was measured using a benchtop salinometer (Orion Star™ A12, Thermo Scientific), which was calibrated using MilliQ water and known salinity CRM seawater each time before sample analysis. The salinometer was also regularly calibrated with 0.5 M KCl at 25°C. Ca^{2+} concentration was determined by potentiometric titration (Kanamori and Ikegami 1980) using EGTA as the titrant. The end-point was detected using a Metrohm® calcium-selective electrode on a

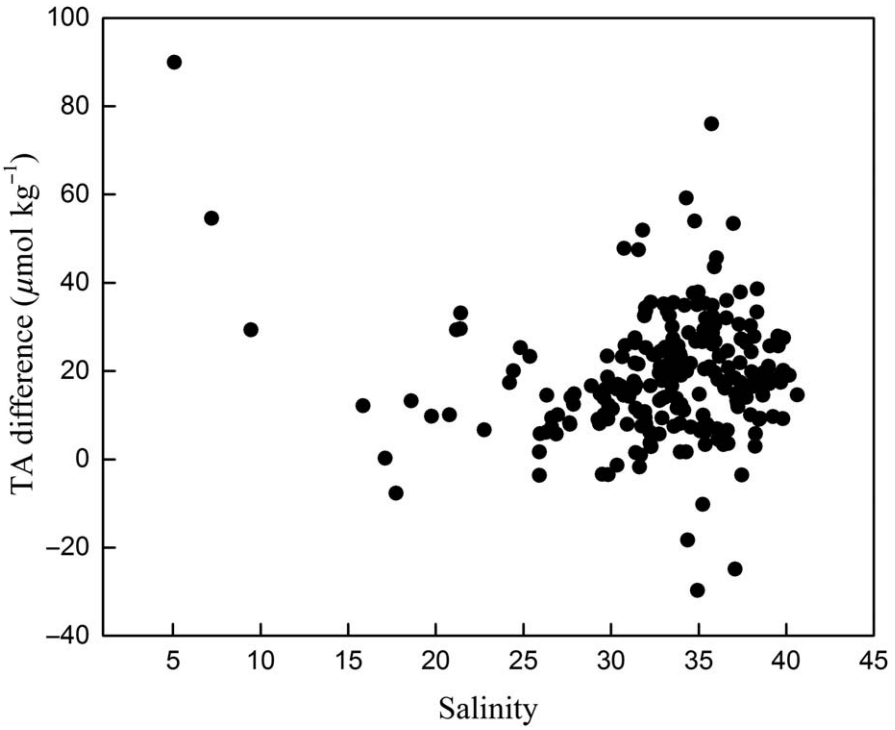

Fig. 2. The difference between measured and calculated TA (from pH and DIC) and its relationship with salinity.

semi-automated titration system. This method had a precision of ± 0.5% for estuarine waters.

Water pCO_2 and Ω_{ar} at field conditions were calculated using the program CO2SYS (Lewis and Wallace, 1998) based on DIC and lab measured pH. We used measured pH and DIC as input variables instead of the pH/TA combination to calculate $pCO_{2,water}$ to avoid possible errors that were resulted from organic alkalinity component (Abril et al. 2015). In fact, we found that the difference between titration alkalinity and calculated alkalinity (with pH and DIC) showed strong salinity dependence in the MAE (Fig. 2). Although calculated $pCO_{2,water}$ was subject to some degree of uncertainty, previous studies showed an 1 : 1 linear relationship between measured and calculated $pCO_{2,water}$ over a range of 300–4000 μatm in estuarine and coastal waters (Frankignoulle and Borges 2001).

Calculated Ω_{ar} from CO2SYS output was corrected using measured Ca^{2+} concentration, which was a near perfect linear function of salinity throughout the year ($r^2 = 0.99$, data not shown). Carbonic acid dissociation constants (K_1, K_2) in Millero (2010), bisulfate dissociation constant in Dickson (1990) were used in this calculation. In the MAE (http://missionaransas.org/science/download-data), the soluble reactive phosphorous concentration was on the order of $\sim$ 2.0 μmol kg^{-1} or less, and silicate concentration was on the order of $\sim$ 200 μmol kg^{-1}. The effect of nutrients on calculated Ω_{ar} and pCO_2 was minimal. For example, pCO_2 would only differ by 0.2 μatm with or without nutrients in the CO2SYS program. Because not all water samples that were characterized for carbonate chemistry had concurrent nutrient information, nutrients were omitted in all carbonate speciation calculations.

Air–water CO_2 flux calculation

The air–water flux of CO_2 was calculated using the following equation:

$$F = kK_0\left(pCO_{2,water} - pCO_{2,air}\right) \quad (2)$$

where k ($m \cdot d^{-1}$) is the gas transfer velocity calculated from wind speed, K_0 ($mol \cdot m^{-3} \cdot atm^{-1}$) is the gas solubility at measured in situ temperature and salinity (Weiss 1974), $pCO_{2,water}$ and $pCO_{2,air}$ are partial pressure of CO_2 in surface water and the atmosphere, respectively. Positive F value means CO_2 degassing to the atmosphere. $pCO_{2,air}$ can be calculated from:

$$pCO_{2,air} = xCO_{2,air} \times (P_b - P_w) \quad (3)$$

Here P_b (atm) is the barometric pressure, which was downloaded from the weather station at Copano East (CE), P_w (atm) is the water vapor pressure calculated using salinity and temperature (Weiss and Price 1980), and $xCO_{2,air}$ (ppm) is the mole fraction atmospheric CO_2 in dry air. We did not measure air xCO_2 directly but chose to download monthly averaged xCO_2 data from http://www.esrl.noaa.gov/gmd/ccgg/trends. We recognized the spatial difference in xCO_2 on

the global scale. However, compared to the xCO_2 data from a coastal CO_2 monitoring site in eastern GOM (https://www.pmel.noaa.gov/co2/story/Coastal + MS), monthly average xCO_2 is no more than 15 ppm greater in the GOM than the Mauna Loa site in winter and the two xCO_2 records generally agree with each other to within ± 2 ppm in summer. Therefore the subsequently calculated CO_2 flux would differ by a few percent using either xCO_2 record (or the actual xCO_2 at MAE). Given that the GOM site does not have a continuous dataset, we used the Mauna Loa data for our calculation.

Gas transfer velocity (k) would differ depending on wind speed, tidal current, and bottom topography (Wanninkhof 1992; Raymond and Cole 2001). Unfortunately, there is no widely accepted k formulation in shallow estuary regions, and the carbon cycle community still has to rely on wind speed dependence to estimate gas exchange rates. Because the equation in Raymond and Cole (2001) was mainly based on relatively low wind speed (< 7 $m \cdot s^{-1}$) estuarine data, here we used the equation in Jiang et al. (2008), which covered larger amount of high wind speed data (up to 12 $m \cdot s^{-1}$) and was more appropriate to our studied area:

$$k = (0.314 \cdot U^2 - 0.436 \cdot U + 3.99) \times (Sc_{SST}/600)^{-0.5} \quad (4)$$

where U is the wind speed at 10-m height ($m \cdot s^{-1}$), Sc_{SST} indicates Schmidt number of CO_2 at the in situ temperature from the freshwater (flooding period) and seawater (drought period) equations, respectively (Wanninkhof 1992). This equation has also been adopted in recent estuarine studies (Bozec et al. 2012; Crosswell et al. 2012).

The total surface area of Aransas and Copano bays is 452 km^2 based on Texas Water Development Board (TWDB) record. Aransas Bay occupies 181 km^2 with estimated 10% of its area in the Aransas Ship Channel where the station SC is located, and Copano Bay is 271 km^2. There is no published record on the area of Mesquite Bay. We estimated its area using a closet rectangle on Google Earth® and calculated its area as 75 km^2. Due to relatively limited sampling stations, we decided to use area-weighted average method to calculate CO_2 flux in the MAE instead of taking arithmetic mean of the individual stations. Our results showed that the difference between these two methods for each trip was 2.5 ± 7.0 $mmol \cdot C \cdot m^{-2} \cdot d^{-1}$, and integrated annual CO_2 flux is 12.4 $mol \cdot C \cdot m^{-2} \cdot yr^{-1}$, compared with 11.4 $mol \cdot C \cdot m^{-2} \cdot yr^{-1}$ using the arithmetic mean. We first calculated area-weighted CO_2 flux using CO_2 flux values at the five sampling stations and the respective areas above. Then to estimate seasonally (drought and flooding periods) or annually averaged CO_2 flux, we used the following equation:

$$F_{avg} = \frac{\sum F_i \times d_i}{\sum d_i} \quad (5)$$

F_{avg} is area-weighted CO_2 flux and has a unit of $mmol \cdot C\ m^{-2} \cdot d^{-1}$ or $mol \cdot C\ m^{-2} \cdot yr^{-1}$, F_i is air–water CO_2 flux of each sampling trip, d_i indicates days in between two consecutive trips. Note in our CO_2 flux calculations we did not consider diel effect. Given that our sampling always took place during the middle of the day (09:00–14:00 h) when pCO_2 was likely the lowest due to photosynthesis, calculated fluxes may represent lower estimates of the actual values (Baumann et al. 2014).

Thermal and non-thermal effects on pCO_2 variations

Thermal and non-thermal effects on $pCO_{2,water}$ variations were evaluated using the method in Takahashi et al. (2002, Eqs. 5–9). To remove the temperature effect, we normalized $pCO_{2,water}$ to annual mean temperature of 23.0°C (T_{mean}, Eq. 6). In surface seawater pCO_2 doubles for every 16°C increase in the oceanic waters ($\partial \ln pCO_2/\partial T = 0.0423$; Takahashi et al. 1993). However, the average $\partial \ln pCO_2/\partial T$ of MAE water was calculated to be slightly lower (0.0411 ± 0.0068) than open ocean water. To evaluate the effect of temperature change on pCO_2, we used Eq. 7.

$$pCO_{2,non-thermal} = pCO_{2,obs} \times \exp[\delta \times (T_{mean} - T_{obs})] \quad (6)$$

$$pCO_{2,thermal} = pCO_{2,mean} \times \exp[\delta \times (T_{obs} - T_{mean})] \quad (7)$$

where δ is $\partial \ln pCO_2/\partial T$, subscripts mean and obs stand for annual mean and observed values, respectively.

To understand relative contributions of thermal and non-thermal effects on temporal pCO_2 changes, we applied the following equations:

$$\Delta pCO_{2,thermal} = Max(pCO_{2,thermal}) - Min(pCO_{2,thermal}) \quad (8)$$

$$\Delta pCO_{2,non-thermal} = Max(pCO_{2,non-thermal}) - Min(pCO_{2,non-thermal}) \quad (9)$$

$$T/B = \Delta pCO_{2,thermal}/\Delta pCO_{2,non-thermal} \quad (10)$$

Both $\Delta pCO_{2,thermal}$ and $\Delta pCO_{2,non\text{-}thermal}$ were calculated from the difference between the maximum and the minimum pCO_2 effects during either the drought or the flooding period. The T/B ratio illustrated the relative importance of thermal vs. non-thermal effects. In MAE, non-thermal effect indicated the combination of biogeochemical processes and physical mixing. Thermal effect on surface $pCO_{2,water}$ would exceed non-thermal if T/B ratio was greater than 1; conversely, non-thermal effect would dominate if T/B ratio was less than 1.

Data analysis

A two-factor analysis of variance (ANOVA) was used to test the effects of hydrologic condition and sampling locations on carbonate variables and CO_2 fluxes. Probabilities (p) of < 0.05 were considered as significant. Normality and homogeneity of variance were ensured before ANOVA was conducted and there was no need to transform the data.

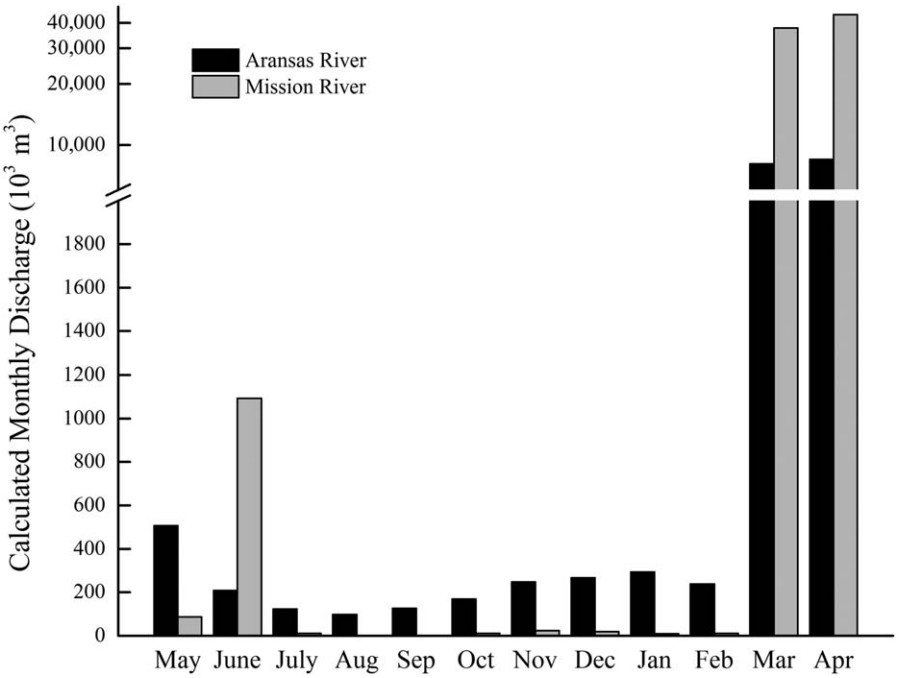

Fig. 3. Monthly freshwater discharges from two major rivers into the MAE from 05/2014 to 04/2015 (data source, USGS).

Results

Hydrologic conditions

During our sampling year, the drought period (05/2014–02/2015,18 trips in total) was much longer than the flooding period (03/2015–04/2015, four trips in total; Fig. 3). Annual discharge for Mission River was 8.29 $\times 10^7$ $m^3 \cdot yr^{-1}$ while discharge for Aransas River was 1.88 $\times 10^7$ $m^3 \cdot yr^{-1}$. Aransas River had more discharge during the drought period (07/2014–02/2015), in which the month with the least discharge was recorded in August 2014 for Aransas and Mission Rivers (97.40 $\times$ 10^3 and 0 m^3 $month^{-1}$, respectively). However, Mission River had more freshwater input during the flooding period (03/2015–04/2015). The MAE was affected by two strong storms in late 03/2015 and 04/2015 (Fig. 3). During this period, Mission River discharge was almost twice as much as Aransas River. The highest discharge from Aransas River (51.25 m^3 s^{-1}) was recorded in 03/2015 and discharge from Mission River was the highest (118.93 m^3 s^{-1}) in 04/2015.

The average values of all physical and chemical parameters for the five stations during the drought and the flooding periods are listed in Table 1 and Fig. 4. The average water temperature during our study period was 23.0 ± 6.3°C ($N = 216$), with the highest temperature (average 29.3 ± 0.7°C; $N = 20$) observed in 08/2014 and the lowest (average 10.0 ± 1.0°C; $N = 10$) in 01/2015. High temperatures (> 25°C) lasted from mid-spring to fall (05/2014–10/2014), a period much longer than low temperature conditions (< 15°C, 11/2014, 01/2015 – early 03/2015). Temperature fluctuated between 15°C and 25°C for the remainder of the sampling period (12/2014, late 03/2015 – 04/2015).

During the entire sampling period, average DO concentration was 212.5 ± 33.7 $\mu mol \cdot kg^{-1}$ ($N = 216$, Fig. 4). Higher DO concentrations occurred during cold months (11/2014 ~ 02/2015). Slight DO stratification occurred in Copano Bay (CW and CE) mostly in spring and summer. In particular, there was a sharp decrease in DO (from 249.8 $\mu mol \cdot kg^{-1}$ to 70.4 $\mu mol \cdot kg^{-1}$) in CW bottom waters after the first storm event in late 03/2015.

Average salinity was 33.0 ± 5.4 ($N = 216$, Fig. 4) during our sampling period. During the drought period there was a gradient from lowest salinity (33.6 ± 2.2, SC; $N = 35$) in the lower primary bay to highest salinity (36.9 ± 2.4, CW; $N = 36$) in the upper secondary bays. Hypersaline conditions ($S > 36.4$) occurred at all five stations from 06/2014 to 09/2014, and persisted particularly long at CW (late 06/2014–01/2015). In early 09/2014, the average salinity of the entire estuary was 38.7 ± 0.8 ($N = 9$), which was the highest during our study period. On the contrary, during the flooding period, there was a salinity gradient (surface and bottom average) across the estuary from the lowest (18.9 ± 10.4, CW; $N = 8$) to the highest (29.0 ± 3.2, SC; $N = 8$). Salinity stratification was only observed in Copano Bay. Salinity decreased sharply at CW after the flood (from 30.1 to 5.1 for surface water).

Carbonate chemistry

All carbonate system parameters displayed significant spatial (station) and temporal differences (between the drought

Table 1. Physical and chemical conditions of MAE during drought and flooding periods in MAE. D and F indicate drought and flooding period, respectively.

Station	Period	Temp (°C)	Salinity	DO (μmol·kg^{-1})	DO%	pH	DIC (μmol·kg^{-1})	TA (μmol·kg^{-1})	$pCO_{2,water}$ (μatm)	Ω_{ar}
Total	D	23.6 ± 6.6	34.7 ± 2.9	208.0 ± 31.8	97.2 ± 5.23	8.018 ± 0.080	2194.7 ± 156.8	2497.6 ± 172.1	477 ± 49	3.3 ± 0.6
	F	20.4 ± 4.3	24.5 ± 6.6	232.3 ± 34.8	95.1 ± 12.1	8.013 ± 0.149	2132.5 ± 256.8	2333.4 ± 283.1	529 ± 251	2.4 ± 0.7
CW	D	23.4 ± 6.9	36.9 ± 2.4	207.2 ± 29.3	97.9 ± 4.3	8.046 ± 0.042	2271.3 ± 199.3	2626.2 ± 234.5	450 ± 62	3.8 ± 0.9
	F	20.6 ± 4.3	18.9 ± 10.4	221.4 ± 65.0	87.3 ± 23.7	7.909 ± 0.269	1870.9 ± 390.0	2012.4 ± 414.6	709 ± 481	1.5 ± 0.8
CE	D	23.7 ± 6.9	35.0 ± 2.4	206.9 ± 31.7	97.2 ± 5.5	7.960 ± 0.084	2157.9 ± 180.2	2429.2 ± 174.8	542 ± 105	2.9 ± 0.3
	F	20.9 ± 4.7	23.7 ± 5.4	231.9 ± 28.8	97.2 ± 8.8	7.990 ± 0.112	2056.4 ± 136.6	2239.1 ± 134.1	529 ± 180	2.2 ± 0.4
AB	D	23.6 ± 6.6	34.4 ± 2.6	205.5 ± 32.3	95.9 ± 4.8	8.034 ± 0.044	2193.4 ± 94.6	2506.8 ± 77.9	453 ± 50	3.4 ± 0.7
	F	20.3 ± 4.6	26.1 ± 3.8	235.2 ± 24.4	96.8 ± 5.0	8.018 ± 0.064	2237.3 ± 88.4	2445.5 ± 107.6	507 ± 88	2.6 ± 0.4
SC	D	23.9 ± 5.5	33.6 ± 2.2	206.5 ± 28.3	96.3 ± 5.9	8.051 ± 0.069	2103.9 ± 54.5	2402.4 ± 47.4	423 ± 70	3.4 ± 0.4
	F	19.2 ± 4.2	29.0 ± 3.2	243.3 ± 18.6	98.7 ± 6.2	8.109 ± 0.048	2091.0 ± 25.1	2342.6 ± 36.7	368 ± 48	2.9 ± 0.2
MB	D	23.6 ± 7.3	33.6 ± 3.5	214.4 ± 38.2	98.9 ± 5.4	7.998 ± 0.109	2248.8 ± 149.6	2522.7 ± 157.5	521 ± 110	3.2 ± 0.3
	F	20.9 ± 4.5	24.5 ± 4.2	230.1 ± 21.1	95.7 ± 4.2	8.038 ± 0.086	2407.0 ± 52.2	2627.4 ± 50.7	530 ± 106	2.8 ± 0.3

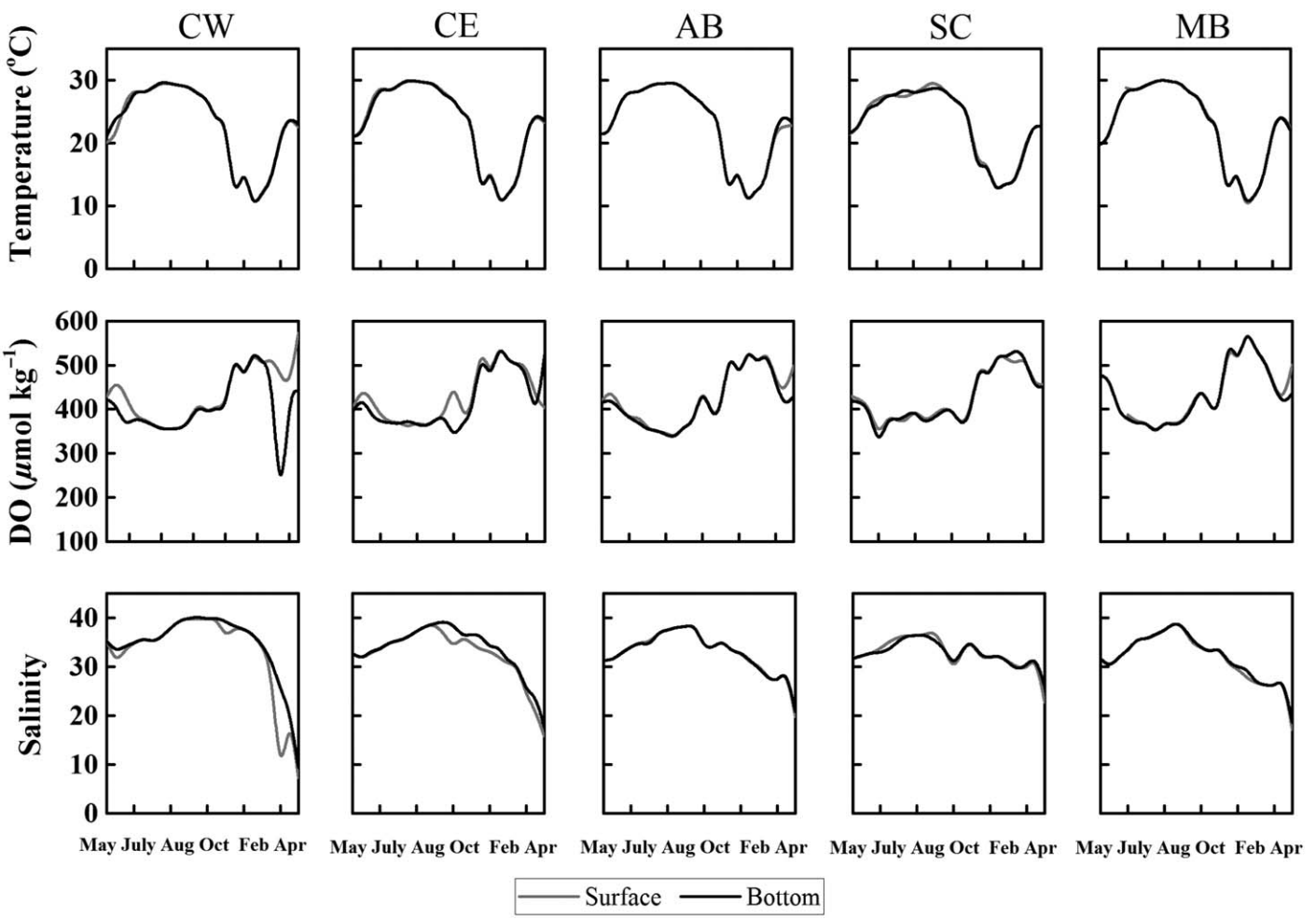

Fig. 4. Seasonal variations of temperature, dissolved oxygen, and salinity in the MAE. The gray and black lines indicate surface and bottom water conditions, respectively.

Table 2. Temporal and spatial analysis of the carbonate system tested by two-way ANOVA. "√" denotes a significant main factor interaction between sampling time (i.e., drought–flooding cycle) and sampling location.

Parameter	Significant interaction	df	*F*	*p*
pH	√	4	5.522	<0.001
DIC	√	4	12.124	<0.001
TA	√	4	18.060	<0.001
$pCO_{2,water}$	√	4	6.430	<0.001
Ω_{ar}	√	4	11.953	<0.001

Both main factors (drought vs. flooding, sample stations) were significant.

and flooding periods) with two-way ANOVA p values < 0.001 for all cases (Table 2). Average pH in MAE was 8.017 ± 0.096 ($N = 216$) with relatively small seasonal and spatial variations compared with many estuarine studies to date. Nevertheless, pH was generally lower (average 7.983 ± 0.064; $N = 49$) when the temperature was high from late 07/2014 to 09/2014, during hypersaline conditions. Higher pH values (average 8.114 ± 0.046; $N = 50$) were observed at low temperature conditions from 11/2014 to early 03/2015, although pH decreased when the estuary switched from the drought to the flooding period, and a very sharp decline of pH at CW ($\Delta = -0.536$ pH units) occurred right after the late 03/2015 storm event.

Annual DIC concentration averaged at 2183.2 ± 180.4 $\mu mol \cdot kg^{-1}$ ($N = 216$, Fig. 5). Average DIC concentration was 2194.7 ± 156.8 $\mu mol \cdot kg^{-1}$ ($N = 176$) during the drought period, and was lower from summer to early fall (2106.8 ± 100.6 $\mu mol \cdot kg^{-1}$, 06/2014–10/2014; $N = 109$) but higher in winter (2230.6 ± 96.0 $\mu mol \cdot kg^{-1}$, 11/2014–02/2015; $N = 40$). CW had the highest DIC concentration and SC had the lowest in drought condition. DIC concentrations during the flooding period (with an average of 2132.5 ± 256.8 $\mu mol \cdot kg^{-1}$; $N = 40$) were lower than the drought period. There was a large decrease in the surface waters at CW after the first storm event in late 03/2015 with DIC concentrations decreasing from 2239.4 $\mu mol \cdot kg^{-1}$ (prior to the storm) to 1227.3 $\mu mol \cdot kg^{-1}$ (after the storm). During the flooding period, MB had the highest DIC concentration, CW the lowest. Along with salinity stratification in Copano Bay during the flooding period, DIC concentration was lower in surface waters than the bottom water.

TA followed a temporal pattern similar to DIC (Fig. 5). Average TA concentration was 2467.2 ± 206.7 $\mu mol \cdot kg^{-1}$ ($N = 216$) across the five stations during the entire sampling period. Average TA concentration was 2497.6 ± 172.1 $\mu mol \cdot kg^{-1}$ ($N = 176$) and 2333.4 ± 283.1 $\mu mol \cdot kg^{-1}$ ($N = 40$) during the drought and the flooding period, respectively.

For the entire estuary, average $pCO_{2,water}$ was 487 ± 138 μatm ($N = 216$, Fig. 5). It was 477 ± 94 μatm ($N = 176$) during the drought period, and 529 ± 251 μatm ($N = 40$) during the flooding period. During the drought period, the highest average $pCO_{2,water}$ occurred at CE (542 ± 105 μatm, $N = 36$) and lowest at SC (423 ± 70 μatm, $N = 35$). During the flooding period, $pCO_{2,water}$ in most stations increased, and CW had the highest average $pCO_{2,water}$, and SC had the lowest. At the same time, calculated $pCO_{2,air}$ in MAE area during our study period averaged at 391 ± 6 μatm using observed monthly $xCO_{2,air}$ at the Mauna Loa site.

Annual average Ω_{ar} was 3.2 ± 0.7 in the MAE ($N = 216$; Fig. 5). Average Ω_{ar} first increased ($\Delta = 0.7$) and then decreased ($\Delta = -1.4$) in drought season, with both the highest (3.8 ± 0.9 at CW, $N = 36$) and lowest (2.9 ± 0.3 at CE, $N = 36$) average Ω_{ar} values observed in Copano Bay. Average Ω_{ar} decreased significantly during the transition from the drought period (average 3.3 ± 0.6; $N = 176$) to the flooding period (average 2.4 ± 0.7; $N = 40$). During the latter period, SC had the highest Ω_{ar} (2.9 ± 0.2, $N = 8$) value and CW had the lowest (1.5 ± 0.8, $N = 8$).

Air–water CO_2 flux

Average wind speed in the MAE was 6.2 ± 2.6 $m \cdot s^{-1}$ ($N = 17{,}520$, Fig. 6) during our sampled period. The highest average (9.7 ± 0.9 $m \cdot s^{-1}$; $N = 48$) was observed in 08/2014 and lowest (2.1 ± 0.8 $m \cdot s^{-1}$; $N = 48$) was observed in 01/2015. During our study period, higher wind speed was recorded in summer (06/2014–08/2014, average 7.1 ± 2.3 $m \cdot s^{-1}$; $N = 288$) and winter had relatively lower wind speed (12/2014–02/2015, average 3.4 ± 1.6 $m \cdot s^{-1}$; $N = 143$).

Overall, annual average air–water CO_2 flux was 12.4 ± 3.3 $mol \cdot C \cdot m^{-2} \cdot yr^{-1}$ ($N = 110$, Fig. 6), and the entire estuary released CO_2 during most of our sampled period. Further, the air–water CO_2 flux pattern displayed significant seasonal and spatial variations ($p < 0.05$ tested by two-way ANOVA; Fig. 6). Throughout the drought period, air–water CO_2 flux varied between -13.5 ± 7.6 $mmol \cdot C \cdot m^{-2} \cdot d^{-1}$ and 109.4 ± 71.3 $mmol \cdot C \cdot m^{-2} \cdot d^{-1}$ (02/2015 and 08/2014, respectively; $N = 5$ for each average value). The estuary was a CO_2 source in the drought period during warm months (05/2014–10/2014) and was a sink during cold months (11/2014–02/2015). Moreover, there was an overall increase in CO_2 efflux from the drought to the flooding period mostly due to large increase of CO_2 emission at CW. In particular, there was a drastic increase (from 3.4 $mmol \cdot C \cdot m^{-2} \cdot d^{-1}$ to 380.3 $mmol \cdot C \cdot m^{-2} \cdot d^{-1}$) at CW in late 03/2015 right after the first storm event.

Discussion

DIC and TA dynamics during the dry-wet cycle

Many Texas rivers have high levels of bicarbonate ion (HCO_3^-) as a result of high weathering rates of the drainage basins (Zeng et al. 2010) and generally high evaporation

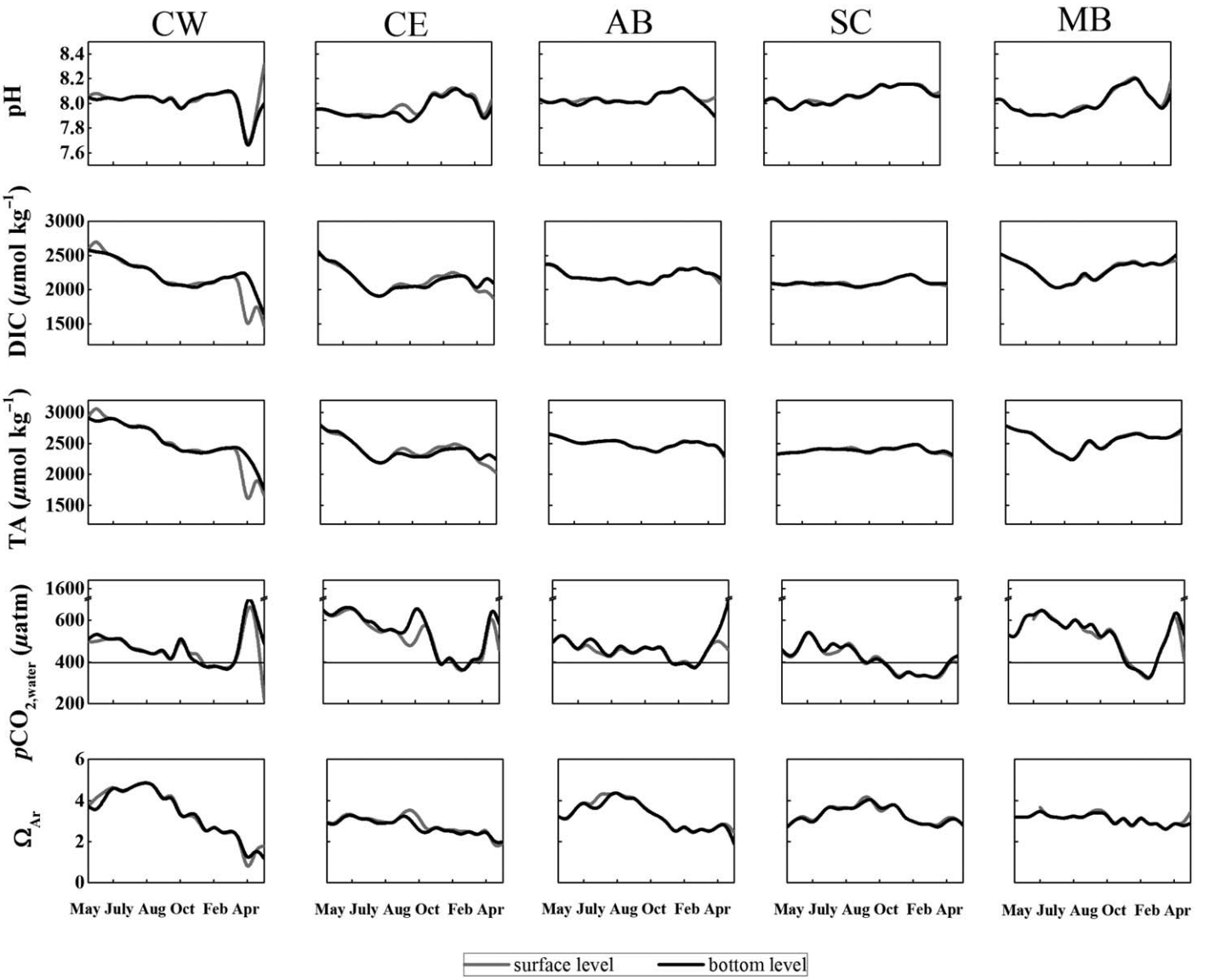

Fig. 5. Seasonal variations of pH (total scale), DIC, TA, $pCO_{2,water}$, and Ω_{ar} in MAE. The gray and black lines indicate surface and bottom water conditions, respectively, and the straight lines in the pCO_2 panels indicates $pCO_{2,air}$.

rates in the area (http://www.twdb.texas.gov/surfacewater/conditions/evaporation/). To unravel the factors that contributed to estuarine DIC and TA variations, we used the water chemistry data to construct two-endmember mixing diagrams for DIC and TA in the MAE during the drought and flooding periods, respectively (Figs. 7,8); we also investigated the effect of precipitation and evaporation. Note for the river endmembers, we did not take river endmember during the 2014–2015 boat trips. Since we did not have concurrent river chemistry data during our estuarine sampling period, to best estimate the river chemistry during the flooding and drought conditions, we collected river samples at Mission and Aransas rivers bimonthly between December 2015 and December 2016 (Table 3). Six trips were conducted during a drought period, and one trip was conducted at the end of May 2016 after significant flooding in south Texas.

As discussed in Hu et al. (2015), along a river-ocean mixing line, the lowest solute to salinity ratio (i.e., the slope of the evaporation line) would be at the ocean endmember if there were no reactions that consumed this solute. Clearly, all the data points to the right of the dotted line (i.e., the precipitation–evaporation line for seawater endmember, Fig. 7) during the drought period reflected net removal of DIC (panels *a*, *b*, and *c*) and TA (panels *d*, *e*, and *f*), and the Copano Bay stations (CE and CW) also showed larger extent of DIC and TA consumption under hypersaline conditions (panels a and d). Furthermore, because the Mission River

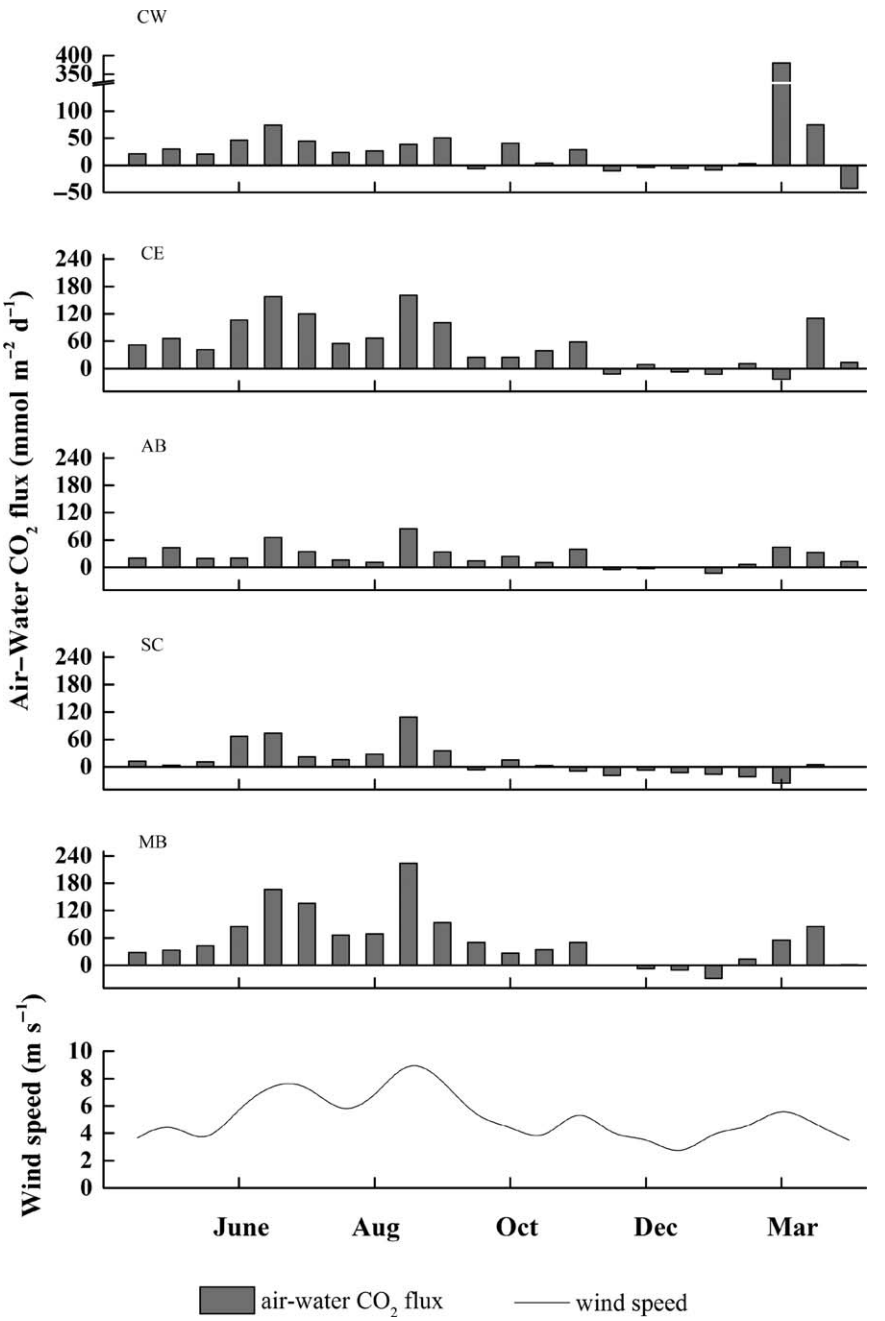

Fig. 6. Air–water CO_2 fluxes at the five stations and wind speed (location) from 05/2014 to 04/2015.

had higher DIC and TA concentrations than the Aransas River (Table 3), the mixing line between the Mission River (the dashed line in Fig. 7) and the ocean water endmember (values in Table 3) should have a slightly steeper slope than that between the Aransas River and the ocean endmember (the solid line in Fig. 7). Therefore, all the data points that are bracketed by the river–ocean mixing lines and the left of the precipitation-evaporation line (to the lower of the plot) also indicated removal.

Normally in an estuarine mixing zone, data points that appear above a mixing line would indicate in situ production as many estuarine studies have indicated (Raymond et al. 2000). However, for lagoonal estuaries with prolonged residence time under drought conditions (Montagna et al. 2012), significant evaporation could increase solute concentration and salinity simultaneously based on the original river–ocean mixing line (*see* Hu et al. 2015 for a detailed discussion). Therefore, it is likely that evaporation may have

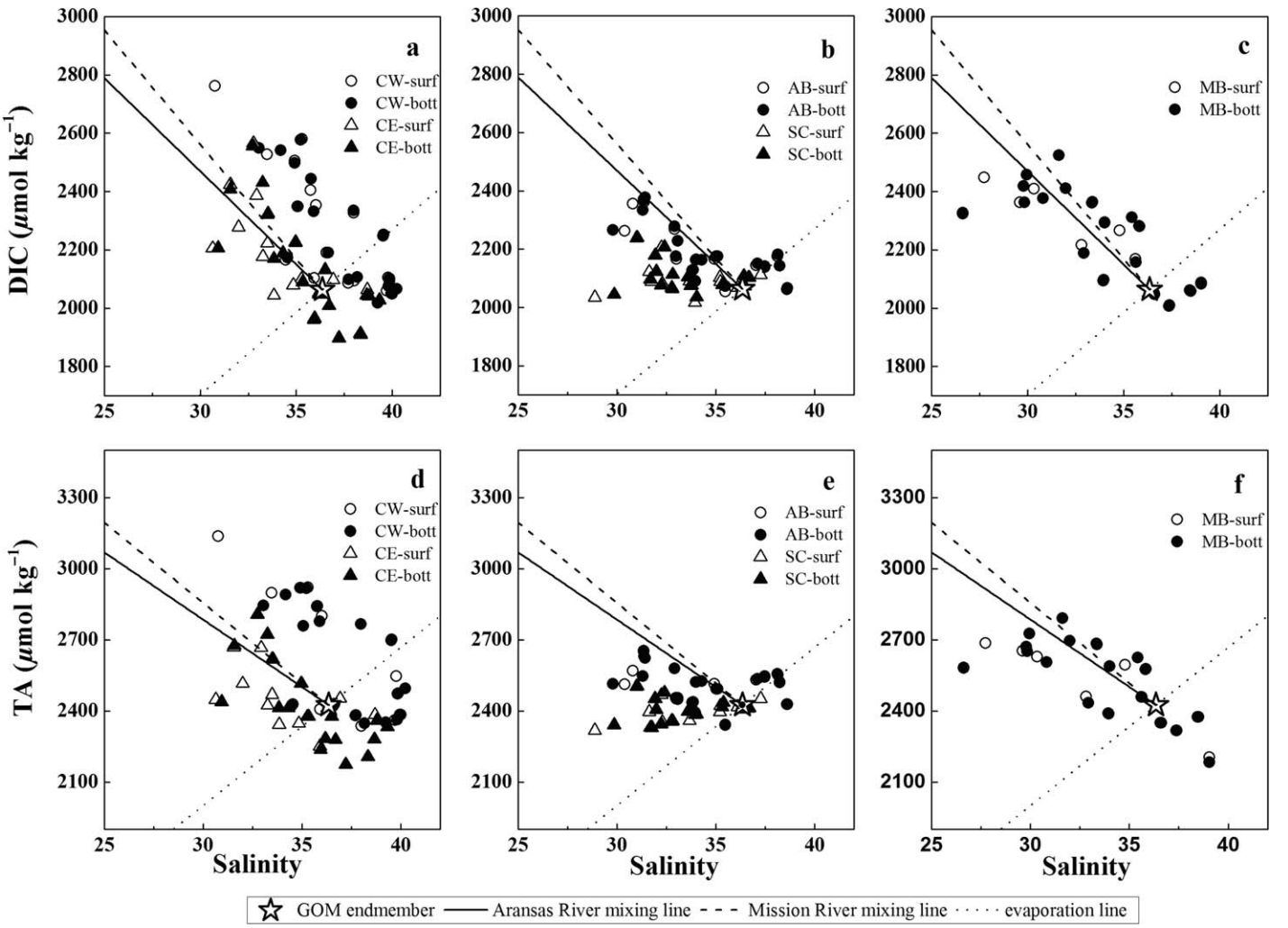

Fig. 7. DIC, TA vs. salinity during the drought period (05/2014–02/2015) in Copano Bay (a and d), Aransas Bay (b and e), and Mesquite Bay (c and f), respectively. The solid and dashed lines represent mixing lines between Aransas and Mission rivers and the Gulf of Mexico (GOM) coastal water, respectively, and the dotted line represents the evaporation line of the GOM coastal water.

played an important role in the water chemistry during the drought period (Fig. 7a,d). Our results could not rule out in situ production of DIC and TA in Copano Bay, although as one moves to Aransas Bay, consumption clearly dominated DIC and TA changes (Fig. 7b,e).

In the literature, alkalinity reduction has not been commonly reported in coastal estuaries (other than in coral reefs). Instead, alkalinity production due to net anaerobic reactions (pyrite burial and net denitrification) is often suggested as an important process (Dollar et al. 1991; Smith et al. 1991; Hu and Cai 2011). Alkalinity consumption due to calcification clearly is a possible mechanism as the MAE has abundant oyster reefs, representing the southernmost location for viable commercial production (Pollack et al. 2012). While not directly observed in the MAE, sulfate concentration in the adjacent Corpus Christi Bay immediately to the south of the MAE appeared to show excess relative to a conservative mixing during the drought period (D. Murgulet pers. comm.), indicating possible external reduced sulfur contribution that was oxidized to sulfuric acid. In addition, Benoit et al. (1994) also observed high levels suspended matter that contains Fe in San Antonio Bay and Corpus Christi Bay, both of which "bracket" the MAE. It is known that oxidation of reduced sulfur and iron would produce H^+ that titrates TA (Chen 2002). Given the shallow depth of the MAE and windy conditions in this area, significant benthic contribution (i.e., reoxidation of reduced sedimentary compounds) is likely, especially during high wind conditions that could cause abundant sediment resuspension. More detailed studies, such as examining sulfur and metal dynamics under different hydrologic conditions, are needed.

During the flooding period, DIC and TA concentrations in the river endmembers decreased (Table 3) presumably due to the dilution effect. Apparently, it became more difficult to explain the DIC and TA variations using the simple mixing

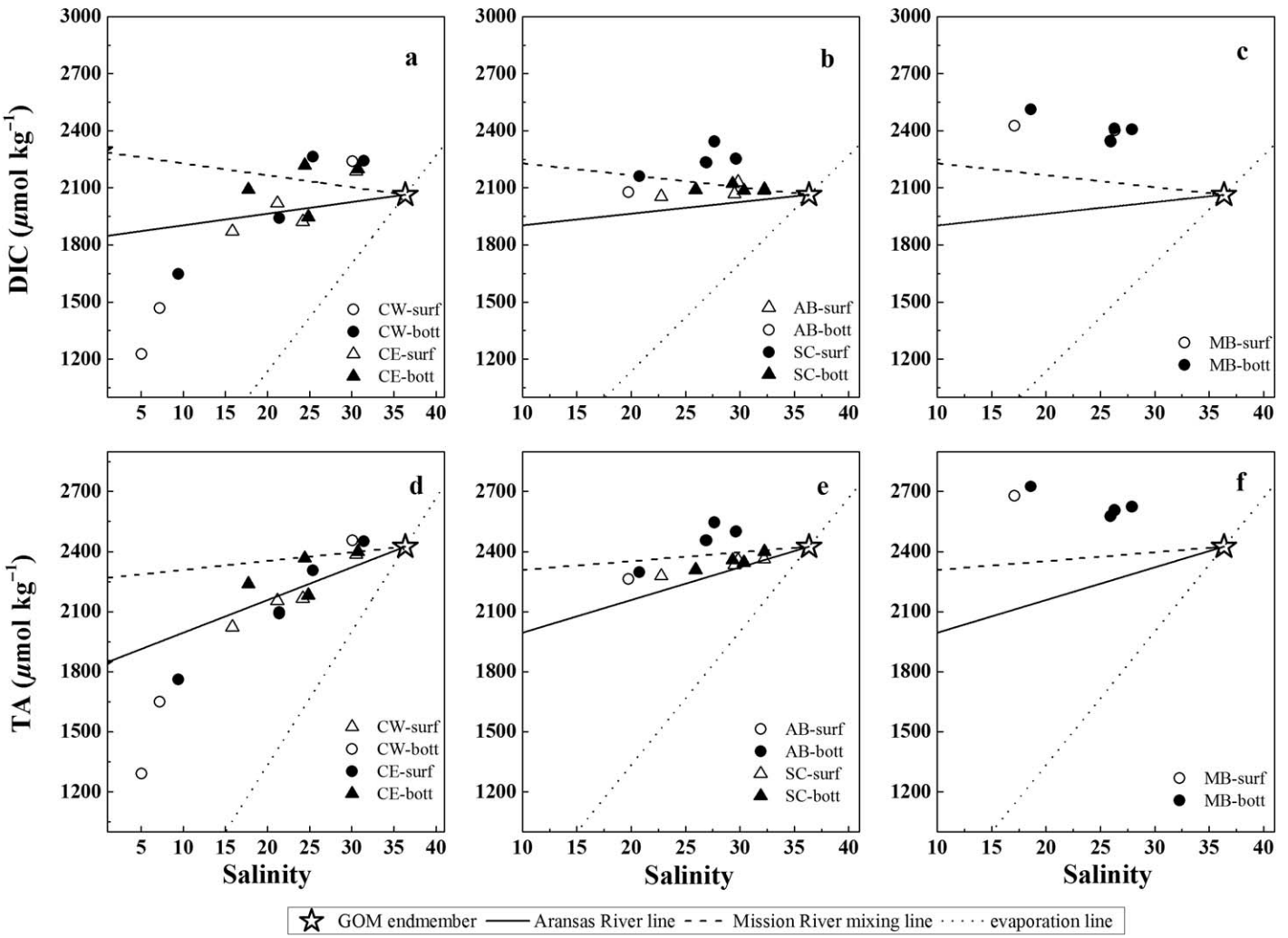

Fig. 8. DIC, TA vs. salinity during the flooding period (03/2015–04/2015) in Copano Bay (a and d), Aransas Bay (b and e), and Mesquite Bay (c and f), respectively. The solid and dashed lines represent mixing lines between Aransas and Mission rivers and the Gulf of Mexico (GOM) coastal water, respectively, and the dotted line represents the evaporation line of the GOM coastal water.

Table 3. Salinity, DIC, TA in the riverine and oceanic input endmembers.

		Aransas River		Mission River	
	GOM*	Drought ($N = 6$)	Flooding	Drought ($N = 6$)	Flooding
Salinity	36.4 ± 0.3	0.7 ± 0.1	0.1	0.7 ± 0.2	0.1
DIC (μmol·kg^{-1})	2063.4 ± 11.4	4345.1 ± 509.2	1841.7	4856.7 ± 761.5	2291.3
TA (μmol·kg^{-1})	2424.6 ± 12.7	4450 ± 542.0	1832.9	4843.1 ± 798.8	2265.0

* Gulf of Mexico endmember was the average of the upper 30 m water column on the Texas shelf ($N = 106$; Hu, unpublished data); river end member was decided by our survey between December 2015 and December 2016, in which six trips were taken in drought periods and one trip was taken in wet period with similar water discharge condition based on the USGS gages data.

lines derived from the local rivers. However, a closer examination of the CW station data suggested that both surface (TA and DIC) and bottom waters (TA only) showed excellent mixing behavior while DIC in the bottom water showed slight respiration signal during the 2-month floodwater-dominated period. For example, intercepts of TA-salinity regressions were 1207 μmol kg^{-1} ($r^2 = 0.95$) for surface and 1449 μmol kg^{-1} ($r^2 = 0.99$) for bottom water respectively; those of DIC-salinity regressions were 1123 μmol kg^{-1} ($r^2 = 0.98$) for surface and 1374 μmol kg^{-1} ($r^2 = 0.89$) for

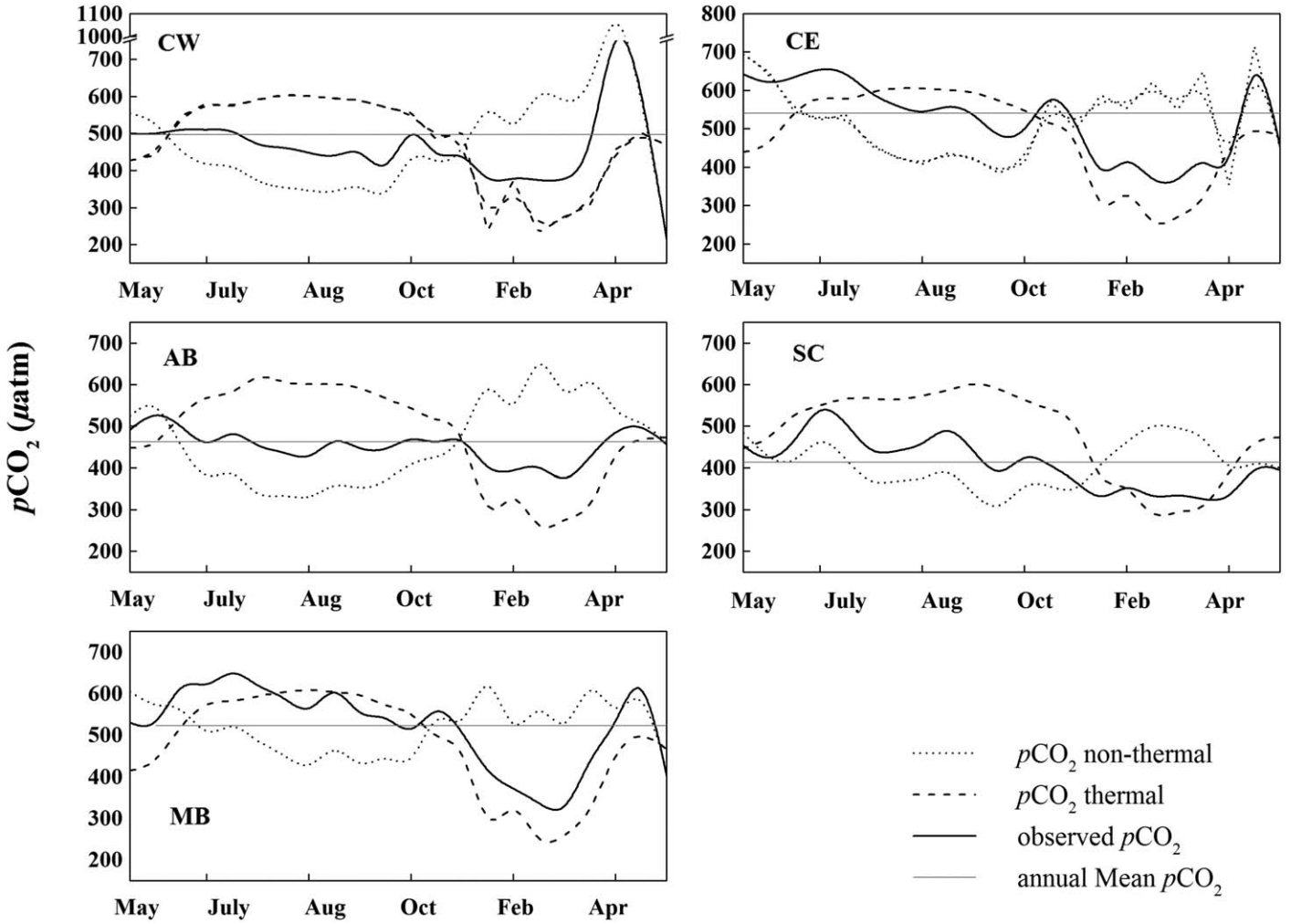

Fig. 9. Seasonal variations of observed $pCO_{2,water}$ ($pCO_{2,obs}$), thermal pCO_2 ($pCO_{2,thermal}$), and non-thermal pCO_2 ($pCO_{2,non\text{-}thermal}$). The horizontal lines represent annual average values.

bottom water, respectively (Fig. 8a,d, regression lines not shown). Therefore, the stagnant endmember values (Table 3) were likely not accurate during the high freshwater inflow season, and the different regression intercepts between the surface and bottom waters may reflect changing freshwater endmember compositions (Cifuentes et al. 1990). Furthermore, Mesquite Bay (MB) (surface and bottom) and the Aransas Bay (bottom) showed "excess" DIC and TA compared to the river mixing line (Fig. 8b,c,e,f). This was likely caused by overflow of high alkalinity San Antonio River (up to 5500 μmol kg^{-1}, Hu, unpublished data) water through Mesquite Bay (Evans et al. 2015) during the flooding period. This high alkalinity water influence decreased from Mesquite Bay to Aransas Bay.

Controlling factors on the $pCO_{2,water}$ variations during the dry–wet cycle

Carbonate system speciation in estuarine waters is controlled by various factors such as temperature, biological processes (primary production, calcification, etc.), and river–ocean mixing (Bozec et al. 2012; Hu and Cai 2013; Hunt et al. 2014; Joesoef et al. 2015). Here we evaluated the effect of temperature and riverine inputs during the drought and flooding periods.

During the drought period, the mean amplitude of thermal effect on water pCO_2 ($pCO_{2,thermal}$–$pCO_{2,water}$) was $\sim$ 190 μatm, which was partially compensated ($\sim$ 100 μatm) by counteractive non-thermal effect ($pCO_{2,non\text{-}thermal}$–$pCO_{2,water}$), thus a net $\sim$ 100 μatm of seasonal amplitude on $pCO_{2,water}$ was observed when there was a warming effect from spring to summer or a cooling effect from summer to winter (Fig. 9). During the flooding period however, mean thermal effect declined to $\sim$ 90 μatm as water temperature increased slightly in 03/2015, whereas there was a large fluctuation of non-thermal effect in 03/2015–04/2015. In particular, sharp increases in $pCO_{2,water}$ was observed in Copano Bay (CW and CE, respectively, Fig. 9), and $pCO_{2,non\text{-}thermal}$ reached its

Table 4. Thermal vs. non-thermal effects on pCO_2 variations in MAE.

		$\Delta pCO_{2,thermal}$ (μatm)		$\Delta pCO_{2,non\text{-}thermal}$ (μatm)		T/B	
Bay	Station	Drought	Flooding	Drought	Flooding	Drought	Flooding
Copano Bay	CW	371	194	335	991	1.11	0.20
	CE	379	206	309	361	1.23	0.57
Aransas Bay	AB	399	185	391	180	1.02	1.02
	SC	339	181	221	101	1.53	1.79
Mesquite Bay	MB	389	208	277	245	1.40	0.85

Table 5. Air–water CO_2 fluxes in different estuaries.

	Average air–water CO_2 flux (*unit*: mol·C·m^{-2}·yr^{-1} for annual; mmol· C·m^{-2}·d^{-1} for seasonal)						
Estuary	Annual	Spring (Mar–May)	Summer (Jun–Aug)	Fall (Sep–Nov)	Winter (Dec–Feb)	Latitude	Reference
[a]Kennebec (US)	3.5 ± 1.0	31.7	–	–	−11.5	44°48′ N	Hunt et al. (2011)
[a]Delaware (US)	2.4 ± 4.8	−13.7 ± 16.4	13.4 ± 22.2	2.7 ± 6.6	15.6 ± 5.2	38°42′–39°18′ N	Joesoef et al. (2015)
[a]Neuse River (US)	4.7	1.73	−0.84	38.4	12.1	34°40′–35°30N	Crosswell et al. (2012)
[b]Florida Bay (US)	1.7	–	–	–	–	25°N	Millero et al. (2001)
[b]Kaneohe Bay (US)	1.5	–	–	–	–	21°24N	Fagan and Mackenzie (2007)
[b]Loire (FR)	8.3 ± 15.5	–	–	–	–	46°30′–47°30′ N	de la Paz et al. (2010)
[b]Changjiang (CN)	−1.9 ± 1.3	−8.8 ± 5.8	−4.9 ± 4.0	2.9 ± 2.5	−10.4 ± 2.3	29°30′–32°30′ N	Zhai and Dai (2009)
[b]Pearl River (CN)	6.9 ± 2.6	12.2∼79.4	5.3∼108.2	15.4∼24.9	−1.09∼22.6	21°30′–23°30′ N	Guo et al. (2009)
[b]Chalakudi (IN)	4.7	–	12.86	–	–	10°41N	Sarma et al. (2012)
[b]Piaui River estuary (BR)	15.0	–	–	–	–	11°30S	Souza et al. (2009)
[a]Mission-Aransas (US)	12.4 ± 3.3	41.8 ± 35.0	74.5 ± 41.1	23.8 ± 16.4	−8.9 ± 5.1	27°50′–28°08′ N	This study

Superscripts a,b indicate different tidal types, a - microtidal estuary and b - macrotidal estuary.

highest concentration (1211 μatm) when the first storm came in late 03/2015. These increases indicated that the storm event caused a dramatic increase in non-thermal pCO_2 (biological and/or mixing). According to Bruesewitz et al. (2013), community respiration in Copano Bay would greatly increase following a storm (thus increasing pCO_2). In addition, high river inflow resulted from storm event also brought in high pCO_2 water. The appearance of peak $pCO_{2,non\text{-}thermal}$ (715 μatm, early 04/2015) was delayed at CE compared to CW (Fig. 9) and the value was lower, indicating that the non-thermal effect became less pronounced with freshwater inflow propagating along the estuary.

Overall, thermal effect dominated the drought period from 05/2014 to 02/2015 for all stations except in AB (Table 4), where thermal and non-thermal effects were about the same. However, during the flooding period, Copano and Mesquite Bay had much lower T/B ratio, indicating that non-thermal effect played a dominant role in controlling $pCO_{2,water}$ variation, consistent with the discussion above. In addition, AB and SC exhibited similar T/B ratios across the dry/wet cycle, indicating that hydrologic state probably did not have a significant effect on the relative importance of thermal vs. non-thermal effect, at least during our sampled time. Considering that station AB is located in the primary bay that has direct exchange with the GOM through the ship channel, and that both AB and SC had smaller salinity variations during the annual cycle (Table 1), these stations clearly were less influenced by river inflow but more by exchange with the GOM.

Air–water CO_2 flux dynamics and controlling factors during the dry-wet cycle

Although accounting for 41% of world's estuarine area, average CO_2 flux in North American estuaries accounts for only 12% of global estuarine CO_2 emission, at a moderate value of 2.2 mol·C·m^{-2}·yr^{-1}, according to a recent synthesis (Chen et al. 2013). However, the average annual air–water CO_2 flux from MAE reached 12.4 ± 3.3 mol·C·m^{-2}·yr^{-1} based on our study. Even though this flux was consistent with results obtained in a limited number of tropical lagoons

Table 6. Estimated average air–water CO_2 flux (mmol·C·m^{-2}·d^{-1}) distribution in the MAE*.

	Copano Bay		Aransas Bay		Mesquite Bay	
	CW	CE	AB	SC	MB	Average
Drought	18.2 ± 24.2	47.0 ± 53.2	18.7 ± 24.4	11.7 ± 34.5	45.7 ± 64.4	28.3 ± 18.0
Flooding	147.9 ± 218.4	40.9 ± 69.3	28.7 ± 19.5	−15.1 ± 20.3	55.7 ± 36.0	51.6 ± 83.9
Annual	35.7 ± 144.8	46.2 ± 86.0	20.0 ± 37.7	8.1 ± 45.5	47.1 ± 76.4	33.8 ± 9.0

* Two-way ANOVA suggests that both "dry-flooding cycle" and "stations" had significant effect on CO_2 flux, and the two main effects also had significant interaction (df = 4, $F = 2.538$, $p < 0.05$).

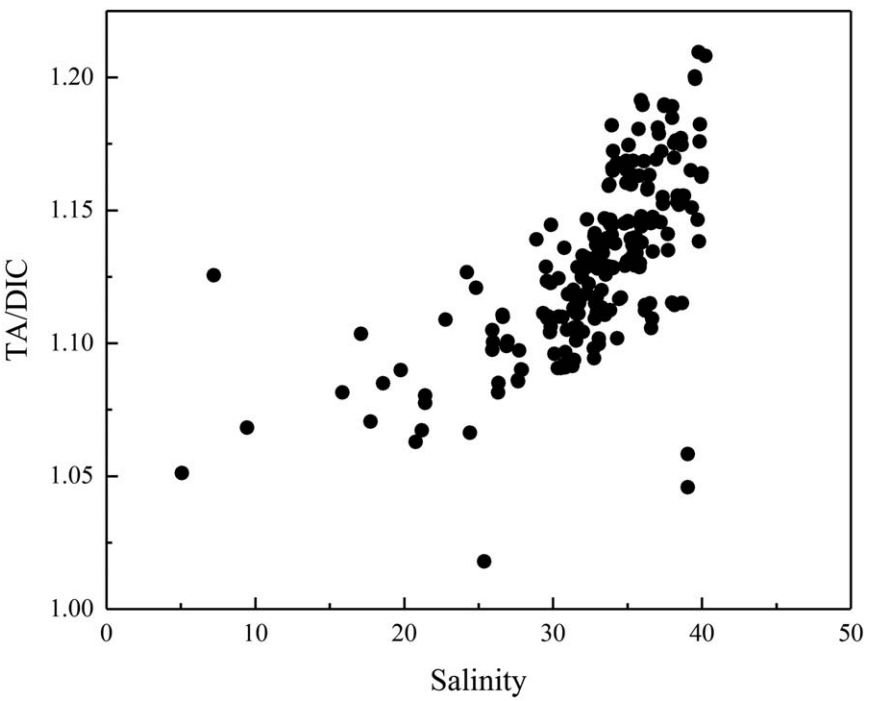

Fig. 10. TA/DIC ratio vs. salinity in the MAE.

(Laruelle et al. 2010), it was significantly higher than many other North American estuaries and even some macrotidal estuaries in Europe (Table 5).

As an important factor that determines gas transfer velocity (Eq. 4), wind speed plays an important role in estuarine CO_2 flux. According to Chen et al. (2013), the mean air–water pCO_2 gradient of European estuaries is only about one third of those in Asian estuaries, whereas the mean air–water CO_2 flux from European estuaries doubled that in Asia due to much higher wind speed. Similarly, despite a relatively low average $pCO_{2,water}$ (487 ± 138 μatm) in MAE compared with much higher $pCO_{2,water}$ in European and Asian estuaries (1600 μatm and 4000 μatm, respectively; Chen et al. 2013), high mean wind speed (5.4 ± 2.3 m·s^{-1}, compared with approximately 4 m·s^{-1} and 1.6 m·s^{-1} on European and Asian coasts, respectively; Chen et al. 2013) contributed to a relatively high CO_2 efflux in this estuary. Therefore, it is desirable to further investigate the role of other low latitude regions, not only within the estuaries, but coastal ocean, in CO_2 budget calculations.

Similar to many other estuaries, air–water CO_2 flux in MAE displayed strong temporal changes during our studied period (Tables 2 and 6). During the drought period, CO_2 emission from the estuary was the highest in summer and early fall (06/2014–09/2014, Fig. 6). This is likely a result of high wind speed (average 6.0 ± 2.4 m·s^{-1}) and high water temperature, and the later could enhance community respiration and evaporation, as more concentrated seawater holds less CO_2. For example, a simulation using CO2SYS suggests that for seawater with salinity 35, total alkalinity 2270 μmol kg^{-1}, total DIC 1977 μmol kg^{-1}, pCO_2 of this seawater would be 400 μatm at 25°C. Then allowing the water evaporate to salinity 40 (hypersaline condition in Copano Bay), pCO_2 would increase to 494 μatm (Fig. 3). If allowing all

"excess" CO_2 to degas and reach equilibrium with the 400 μatm atmosphere, a degassing process that may take only a few days given the shallow water depth here, this evaporation-concentrated water would hold ~ 50 μmol kg^{-1} less DIC than the "concentrated" original seawater. With additional alkalinity reduction, regardless its cause, prolonged water residence time would lead to even more CO_2 loss to the atmosphere. Indeed, TA/DIC ratio in all stations increased with increasing salinity (i.e., average TA/DIC increased from 1.116 ± 0.012 to 1.172 ± 0.024, along with the increase of average salinity from 31.6 ± 1.0 to 38.7 ± 0.8, $N = 10$; Fig. 10). Part of the TA/DIC increase can be attributed to higher TA/DIC ratio in the ocean endmember, and then further depletion of DIC relative to TA toward hypersaline conditions indicated that evaporation contributed to a net CO_2 loss.

Toward the end of the drought period, $pCO_{2,water}$ started to decline with decreasing temperature, and the entire estuary became a weak CO_2 sink from late fall to winter (11/2014–02/2015). Particularly in 02/2015, at all five stations surface water was undersaturated for CO_2 (average $pCO_{2,water} = 341 \pm 49$ μatm). This could be attributed to low riverine input and lower water temperature (Hunt et al. 2014). Note this period also had lower wind speed (average 3.7 ± 0.9 $m \cdot s^{-1}$) thus CO_2 uptake was modest.

CO_2 efflux also displayed spatial variations during our sampling period (Table 6). There was a decreasing trend of average CO_2 emission (46.2–8.1 $mmol \cdot C \cdot m^{-2} \cdot d^{-1}$) from the secondary bays (Copano and Mesquite) to the primary bay (Aransas). Mean air–water CO_2 flux at the ship channel (SC) was the lowest (8.1 ± 34.2 $mmol \cdot C \cdot m^{-2} \cdot d^{-1}$; $N = 22$). This spatial distribution agrees with other estuarine studies as CO_2 efflux typically decreases toward the ocean (Crosswell et al. 2012; Hunt et al. 2014; Joesoef et al. 2015). However, higher CO_2 emission was observed at mid-estuary (CE and MB) especially in the drought period. This was possibly due to more intense remineralization reactions (Table. 1; Fig. 5), which was in favor of CO_2 production. In flooding season, non-thermal effect dramatically increased (Table 4) air–water CO_2 flux at CW, whereas CO_2 degassing was maintained at similar level or even decreased in other part of this estuary, due presumably to nutrient-enhanced primary production (Reyna et al. 2017).

Conclusions

Both carbonate chemistry and CO_2 flux demonstrated substantial temporal and spatial variations in the subtropical MAE, which was affected by strong interannual changes in estuarine hydrologic states. There was a gradient for carbonate variables and CO_2 flux from the secondary bays to the primary bay. We observed significant TA and DIC removal during the drought period and mixing dominated distribution in the flooding season, although detailed mechanisms for the alkalinity loss still await further investigation.

Overall, the MAE was a CO_2 source with an annual average air–water CO_2 flux 12.4 ± 3.3 $mol \cdot C \cdot m^{-2} \cdot yr^{-1}$. High wind speed played an important role for this high CO_2 efflux despite the relatively small air–water pCO_2 gradient. This estimate is much higher than existing, yet scarce, estimates in other subtropical estuaries. During the drought and warm period, CO_2 emission was enhanced by increased temperature (hence increased respiration) and evaporation, and highest CO_2 emission (74.5 ± 41.1; $N = 30$ $mmol \cdot m^{-2} \cdot d^{-1}$) was found in summer in the drought period. However, lower temperature in winter would turn the entire estuary into a weak CO_2 sink (-8.9 ± 5.1 $mmol \cdot m^{-2} \cdot d^{-1}$; $N = 15$). In the flooding period, storm events briefly yet significantly enhanced air–water CO_2 flux at CW due to much elevated pCO_2 level there. Overall, our work suggests that global estuarine CO_2 flux estimates need to be improved by incorporating new studies that focus on subtropical and/or windy estuaries.

References

Abril, G., M. V. Commarieu, D. Maro, M. Fontugne, F. Guérin, and H. Etcheber. 2004. A massive dissolved inorganic carbon release at spring tide in a highly turbid estuary. Geophys. Res. Lett. **31**: L09316. doi:10.1029/2004GL019714

Abril, G., and others. 2015. Technical note: Large overestimation of pCO_2 calculated from pH and alkalinity in acidic, organic-rich freshwaters. Biogeosciences **12**: 67–78. doi:10.5194/bg-12-67-2015

Bauer, J. E., W. J. Cai, P. A. Raymond, T. S. Bianchi, C. S. Hopkinson, and P. A. Regnier. 2013. The changing carbon cycle of the coastal ocean. Nature **504**: 61–70. doi:10.1038/nature12857

Baumann, H., R. B. Wallace, T. Tagliaferri, and C. J. Gobler. 2014. Large natural pH, CO_2 and O_2 fluctuations in a temperate tidal salt marsh on diel, seasonal, and interannual time scales. Estuaries Coast. **38**: 220–231. doi:10.1007/s12237-014-9800-y

Benoit, G., S. D. Oktay-Marshall, A. Cantu, E. M. Hood, C. H. Coleman, M. O. Corapcioglu, and P. H. Santschi. 1994. Partitioning of Cu, Pb, Ag, Zn, Fe, Al, and Mn between filter-retained particles, colloids, and solution in six Texas estuaries. Mar. Chem. **45**: 307–336. doi:10.1016/0304-4203(94)90076-0

Bockmon, E. E., and A. G. Dickson. 2014. A seawater filtration method suitable for total dissolved inorganic carbon and pH analyses. Limnol. Oceanogr.: Methods **12**: 191–195. doi:10.4319/lom.2014.12.191

Bozec, Y., T. Cariou, E. Macé, P. Morin, D. Thuillier, and M. Vernet. 2012. Seasonal dynamics of air-sea CO_2 fluxes in the inner and outer Loire estuary (NW Europe). Estuar. Coast. Shelf Sci. **100**: 58–71. doi:10.1016/j.ecss.2011. 05.015

Bruesewitz, D. A., W. S. Gardner, R. F. Mooney, L. Pollard, and E. J. Buskey. 2013. Estuarine ecosystem function response to flood and drought in a shallow, semiarid estuary: Nitrogen cycling and ecosystem metabolism. Limnol. Oceanogr. **58**: 2293–2309. doi:10.4319/lo.2013.58.6.2293

Cai, W. J. 2011. Estuarine and coastal ocean carbon paradox: CO_2 sinks or sites of terrestrial carbon incineration? Ann. Rev. Mar. Sci. **3**: 123–145 doi:10.1146/annurev-marine-120709-142723

Carter, B. R., J. A. Radich, H. L. Doyle, and A. G. Dickson. 2013. An automated system for spectrophotometric seawater pH measurements. Limnol. Oceanogr.: Methods **11**: 16–27. doi:10.4319/lom.2013.11.16

Chen, C. T. A. 2002. Shelf-vs. dissolution-generated alkalinity above the chemical lysocline. Deep Sea Res. Part II **49**: 5365–5375. doi:10.1016/S0967-0645(02)00196-0

Chen, C. T. A., T. H. Huang, Y. C. Chen, Y. Bai, X. He, and Y. Kang. 2013. Air–sea exchanges of CO_2 in the world's coastal seas. Biogeosciences **10**: 6509–6544. doi:10.5194/bg-10-6509-2013

Cifuentes, L. A., L. E. Schemel, and J. H. Sharp 1990. Qualitative and numerical analyses of the effects of river inflow variations on mixing diagrams in estuaries. Estuar. Coast. Shelf S. **30**: 411–427. doi:10.1016/0272-7714(90)90006-D

Clayton, T. D., and R.H. Byrne. 1993. Spectrophotometric seawater pH measurements: total hydrogen ion concentration scale calibration of m-cresol purple and at-sea results. Deep-Sea Res. Pt. I **40**: 2115–2129. doi:10.1016/0967-0637(93)90048-8

Cross, J. N., J. T. Mathis, N. R. Bates, and R. H. Byrne. 2013. Conservative and non-conservative variations of total alkalinity on the southeastern Bering Sea shelf. Mar. Chem. **154**: 100–112. doi:10.1016/j.marchem.2013.05.012

Crosswell, J. R., M. S. Wetz, B. Hales, and H. W. Paerl. 2012. Air-water CO_2 fluxes in the microtidal Neuse River Estuary, North Carolina. J. Geophys. Res. Oceans **117**: C08017. doi:10.1029/2012jc007925

Crosswell, J. R., M. S. Wetz, B. Hales, and H. W. Paerl. 2014. Extensive CO_2 emissions from shallow coastal waters during passage of Hurricane Irene (August 2011) over the Mid-Atlantic coast of the U.S.A. Limnol. Oceanogr. **59**: 1651–1665. doi:10.4319/lo.2014.59.5.1651

de la Paz, M., X. A. Padín, A. F. Ríos, and F. F. Pérez. 2010. Surface fCO_2 variability in the Loire plume and adjacent shelf waters: High spatio-temporal resolution study using ships of opportunity. Mar. Chem. **118**: 108–118. doi:10.1016/j.marchem.2009.11.004

Dickson, A. G. 1990. Standard potential of the reaction: $AgCl(s) + 12H_2(g) = Ag(s) + HCl(aq)$, and the standard acidity constant of the ion HSO_4^- in synthetic sea water from 273.15 to 318.15 K. J. Chem. Thermodyn. **22**: 113–127. doi:10.1016/0021-9614(90)90074-Z

Dickson, A. G., J. D. Afghan, and G. C. Anderson. 2003. Reference materials for oceanic CO_2 analysis: a method for the certification of total alkalinity. Mar. Chem. **80**: 185–197. doi:10.1016/S0304-4203(02)00133-0

Dickson, A. G., C. L. Sabine, and J. R. Christian. 2007. Guide to best practices for ocean CO_2 measurements. PICES Special Publication 3.

Dollar, S. J., S. V. Smith, S. M. Vink, S. Obrebski, and J. T. Hollibaugh. 1991. Annual cycle of benthic nutrient fluxes in Tomales Bay, California, and contribution of the benthos to total ecosystem metabolism. Mar. Ecol. Prog. Ser. Oldendorf. **79**: 115–125. doi:10.3354/meps079115

Doney, S. C., I. Lima, R. A. Feely, D. M. Glover, K. Lindsay, N. Mahowald, J. K. Moore and R. Wanninkhof. 2009. Mechanisms governing interannual variability in upper-ocean inorganic carbon system and air–sea CO_2 fluxes: Physical climate and atmospheric dust. Deep Sea Res. Part II **56**: 640–655. doi:10.1016/j.dsr2.2008.12.006

Dürr, H. H., G. G. Laruelle, C. M. van Kempen, C. P. Slomp, M. Meybeck, and H. Middelkoop. 2011. Worldwide typology of nearshore coastal systems: Defining the estuarine filter of river inputs to the oceans. Estuaries Coast. **34**: 441–458. doi:10.1007/s12237-011-9381-y

Evans, A., K. Madden, and S. Palmer. 2015. The ecology and sociology of the mission-aransas estuary: An estuarine and watershed profile. University of Texas Marine Science Institute, Port Aransas, Texas.

Fagan, K. E., and F. T. Mackenzie. 2007. Air–sea CO_2 exchange in a subtropical estuarine-coral reef system, Kaneohe Bay, Oahu, Hawaii. Mar. Chem. **106**: 174–191. doi:10.1016/j.marchem.2007.01.016

Feely, R. A., S. R. Alin, J. Newton, C. L. Sabine, M. Warner, A. Devol, C. Krembs, and C. Maloy. 2010. The combined effects of ocean acidification, mixing, and respiration on pH and carbonate saturation in an urbanized estuary. Estuar. Coast. Shelf Sci. **88**: 442–449. doi:10.1016/j.ecss.2010.05.004

Frankignoulle, M., G. Abril, A. Borges, I. Bourge, C. Canon, B. Delille, E. Libert, J.-M. Théate. 1998. Carbon dioxide emission from European estuaries. Science **282**: 434–436. doi: 10.1126/science.282.5388.434

Frankignoulle, M., and A. V. Borges. 2001. Direct and indirect pCO_2 measurements in a wide range of pCO_2 and salinity values (the Scheldt estuary). Aquat. Geochem. **7**: 267–273. doi:10.1023/A:1015251010481

Guo, X., M. Dai, W. Zhai, W.-J. Cai, and B. Chen. 2009. CO_2 flux and seasonal variability in a large subtropical estuarine system, the Pearl River Estuary, China. J. Geophys. Res. **114**: G03013. doi:10.1029/2008jg000905

Hsu, S. A., E. A. Meindl, and D. B. Gilhousen. 1994. Determining the power-law wind-profile exponent under near-neutral stability conditions at sea. J. Appl. Meteorol. **33**: 757–765. doi: 10.1175/1520-0450(1994)033<0757:DTPLWP>2.0.CO;2

Hu, X., and W. J. Cai. 2011. An assessment of ocean margin anaerobic processes on oceanic alkalinity budget. Global Biogeochem. Cycles **25**: GB3003. doi:10.1029/2010GB003859

Hu, X., and W.-J. Cai. 2013. Estuarine acidification and minimum buffer zone-A conceptual study. Geophys. Res. Lett. **40**: 5176–5181. doi:10.1002/grl.51000

Hu, X., J. B. Pollack, M. R. McCutcheon, P. A. Montagna, and Z. Ouyang. 2015. Long-term alkalinity decrease and acidification of estuaries in northwestern Gulf of Mexico. Environ. Sci. Technol. **49**: 3401–3409. doi:10.1021/es505945p

Hunt, C. W., J. E. Salisbury, and D. Vandemark. 2011. Contribution of non-carbonate anions to total alkalinity and overestimation of pCO_2 in New England and New Brunswick rivers. Biogeosciences **8**: 3069–3076. doi:10.5194/bg-8-3069-2011

Hunt, C. W., J. E. Salisbury, and D. Vandemark. 2014. CO_2 input dynamics and air–sea exchange in a large New England estuary. Estuaries Coast. **37**: 1078–1091. doi:10.1007/s12237-013-9749-2

Jiang, L. Q., W. J. Cai, and Y. Wang. 2008. A comparative study of carbon dioxide degassing in river- and marine-dominated estuaries. Limnol. Oceanogr. **53**: 2603–2615. doi:10.4319/lo.2008.53.6.2603

Joesoef, A., W. J. Huang, Y. Gao, and W. J. Cai. 2015. Air–water fluxes and sources of carbon dioxide in the Delaware Estuary: Spatial and seasonal variability. Biogeosciences **12**: 6085–6101. doi:10.5194/bg-12-6085-2015

Kanamori, S., and H. Ikegami. 1980. Computer-processed potentiometric titration for the determination of calcium and magnesium in sea water. J. Oceanogr. Soc. Jpn. **36**: 177–184. doi:10.1007/BF02070330

Kim, H.-C., and P. A. Montagna. 2012. Effects of climate-driven freshwater inflow variability on macrobenthic secondary production in Texas lagoonal estuaries: A modeling study. Ecol. Model. **235–236**: 67–80. doi:10.1016/j.ecolmodel.2012.03.022

Laruelle, G. G., H. H. Dürr, C. P. Slomp, and A. V. Borges. 2010. Evaluation of sinks and sources of CO_2 in the global coastal ocean using a spatially-explicit typology of estuaries and continental shelves. Geophys. Res. Lett. **37**: L15607. doi:10.1029/2010gl043691

Laruelle, G. G., R. Lauerwald, J. Rotschi, P. A. Raymond, J. Hartmann, and P. Regnier. 2015. Seasonal response of air–water CO_2 exchange along the land–ocean aquatic continuum of the northeast North American coast. Biogeosciences **12**: 1447–1458. doi:10.5194/bg-12-1447-2015

Lewis, E., and D. Wallace. 1998. Program developed for CO_2 system calculations, p. 18. ORNL/CDIAC-105.

Liu, X., M. C. Patsavas, and R. H. Byrne. 2011. Purification and characterization of meta-cresol purple for spectrophotometric seawater pH measurements. Environ. Sci. Technol. **45**: 4862–4868. doi:10.1021/es200665d

Millero, F. J. 2001. The physical chemistry of natural waters. Wiley-Interscience.

Millero, F. J. 2010. Carbonate constants for estuarine waters. Mar. Freshw. Res. **61**: 139–142. doi:10.1071/MF09254

Millero, F. J., W. T. Hiscock, F. Huang, M. Roche, and J. Z. Zhang. 2001. Seasonal variation of the carbonate system in Florida Bay. Bull. Mar. Sci. **68**: 101–123.

Milliman, J. D., K. L. Farnsworth, P. D. Jones, K. H. Xu, and L. C. Smith. 2008. Climatic and anthropogenic factors affecting river discharge to the global ocean, 1951–2000. Global Planet. Change **62**: 187–194. doi:10.1016/j.gloplacha.2008.03.001

Montagna, P., T. A. Palmer, and J. Pollack. 2012. Hydrological changes and estuarine dynamics. Springer.

Mooney, R. F., and J. W. McClelland. 2012. Watershed export events and ecosystem responses in the mission–Aransas National Estuarine Research Reserve, South Texas. Estuaries Coast. **35**: 1468–1485. doi:10.1007/s12237-012-9537-4

Pollack, J. B., A. Cleveland, T. A. Palmer, A. S. Reisinger, and P. A. Montagna. 2012. A restoration suitability index model for the eastern oyster (*Crassostrea virginica*) in the Mission-Aransas Estuary, TX, USA. PLoS One **7**: e40839. doi:10.1371/journal.pone.0040839

Raymond, P. A., J. E. Bauer, and J. J. Cole. 2000. Atmospheric CO_2 evasion, dissolved inorganic carbon production, and net heterotrophy in the York River estuary. Limnol. Oceanogr. **45**: 1707–1717. doi:10.4319/lo.2000.45.8.1707

Raymond, P. A., and J. J. Cole. 2001. Gas exchange in rivers and estuaries: Choosing a gas transfer velocity. Estuaries Coast. **24**: 312–317. doi:10.2307/1352954

Regnier, P., and others 2013. Anthropogenic perturbation of the carbon fluxes from land to ocean. Nat. Geosci. **6**: 597–607. doi:10.1038/ngeo1830

Reisdorph, S. C., and J. T. Mathis. 2014. The dynamic controls on carbonate mineral saturation states and ocean acidification in a glacially dominated estuary. Estuar. Coast. Shelf Sci. **144**: 8–18. doi:10.1016/j.ecss.2014.03.018

Reyna, N. E., A. Hardison, and Z. Liu. 2017. Influence of major storm events on the quantity and composition of particulate organic matter and the phytoplankton community in a subtropical estuary, Texas. Front. Mar. Sci. **4**. doi:10.3389/fmars.2017.00043

Sarma, V.V.S.S., and others. 2012. Carbon dioxide emissions from Indian monsoonal estuaries. Geophys. Res. Lett. **39**: L03602. doi:10.1029/2011gl050709

Semesi, I. S., S. Beer, and M. Björk. 2009. Seagrass photosynthesis controls rates of calcification and photosynthesis of calcareous macroalgae in a tropical seagrass meadow. Mar. Ecol. Prog. Ser. **382**: 41–48. doi:10.3354/meps07973

Smith, S. V., J. T. Hollibaugh, S. J. Dollar, and S. Vink. 1991. Tomales bay metabolism: C-N-P stoichiometry and ecosystem heterotrophy at the land-sea interface. Estuar. Coast. Shelf Sci. **33**: 223–257. doi:10.1016/0272-7714(91)90055-G

Souza, M. F., V. R. Gomes, S. S. Freitas, R. C. Andrade, and B. Knoppers. 2009. Net ecosystem metabolism and

nonconservative fluxes of organic matter in a tropical mangrove estuary, Piauí River (NE of Brazil). Estuaries Coast. **32**: 111–122. doi:10.1007/s12237-008-9104-1

Takahashi, T., J. Olafsson, J. G. Goddard, D. W. Chipman, and S. Sutherland. 1993. Seasonal variation of CO_2 and nutrients in the high-latitude surface oceans: A comparative study. Global Biogeochem. Cycles **7**: 843–878. doi: 10.1029/93GB02263

Takahashi, T., and others. 2002. Global sea–air CO_2 flux based on climatological surface ocean pCO_2, and seasonal biological and temperature effects. Deep-Sea Res. Part II **49**: 1601–1622. doi:10.1016/S0967-0645(02)00003-6

Wallace, R. B., H. Baumann, J. S. Grear, R. C. Aller, and C. J. Gobler. 2014. Coastal ocean acidification: The other eutrophication problem. Estuar. Coast. Shelf Sci. **148**: 1–13. doi:10.1016/j.ecss.2014.05.027

Wanninkhof, R. 1992. Relationship between wind speed and gas exchange. J. Geophys. Res. **97**: 7373–7382. doi: 10.1029/92JC00188

Weiss, R. F. 1974. Carbon dioxide in water and seawater: The solubility of a non-ideal gas. Mar. Chem. **2**: 203–215. doi:10.1016/0304-4203(74)90015-2

Weiss, R. F., and B. A. Price. 1980. Nitrous oxide solubility in water and seawater. Mar. Chem. **8**: 347–359. doi:10.1016/0304-4203(80)90024-9

Zeng, F.-W., C. A. Masiello, and W. C. Hockaday. 2010. Controls on the origin and cycling of riverine dissolved inorganic carbon in the Brazos River, Texas. Biogeochemistry **104**: 275–291. doi:10.1007/s10533-010-9501-y

Zhai, W., M. Dai, and X. Guo. 2007. Carbonate system and CO_2 degassing fluxes in the inner estuary of Changjiang (Yangtze) River, China. Mar. Chem. **107**: 342–356. doi: 10.1016/j.marchem.2007.02.011

Zhai, W., and M. Dai. 2009. On the seasonal variation of air – sea CO_2 fluxes in the outer Changjiang (Yangtze River) Estuary, East China Sea. Mar. Chem. **117**: 2–10. doi: 10.1016/j.marchem.2009.02.008

Acknowledgments

We are grateful for the fieldwork assistance provided by the staff and students at both the Mission Aransas National Estuarine Research Reserve and the University of Texas Marine Science Institute. We also thank H. Wang, Q. Liu, Z. Ouyang, and C. J. Staryk for their help with both field sampling and lab analyses, and Lei Jin for the helpful discussion on statistics. The Associate Editor and two anonymous reviewers offered critical comments that helped us to improve the quality of this manuscript significantly. This study was funded by NOAA's NOS National Center for Coastal Ocean Science (Contract No. NA15NOS4780185). Partial funding to this work was provided by the Texas Research Development Fund from the Research and Commercialization Office of Texas A&M University - Corpus Christi. This research was also supported in part by operations grants to the Mission-Aransas National Estuarine Research Reserve from the Office of Coastal Management, National Oceanic and Atmospheric Administration. System-Wide Monitoring Program data were collected by the research staff of the Mission-Aransas NERR and hosted by the Central Data Management Office of the National Estuarine Research Reserve System.

Conflict of Interest

None declared.

Submitted 07 November 2016
Revised 04 April 2017; 01 July 2017
Accepted 10 July 2017

Associate editor: M. Dileep Kumar